NAVAL POSTGRADUATE SCHOOL

MONTEREY, CALIFORNIA

THESIS

THERMOMECHANICAL BEHAVIOR OF MONOLITHIC SN-AG-CU SOLDER AND COPPER FIBER REINFORCED SOLDERS

by

Rolando Reuse

September 2005

Thesis Advisor: Indranath Dutta

Approved for public release, distribution is unlimited

THIS PAGE INTENTIONALLY LEFT BLANK

REPORT DOCUMENTATION PAGE			Form Approved OMB No. 0704-0188
Public reporting burden for this collection of information is estimated to average 1 hour per response, including the time for reviewing instruction, searching existing data sources, gathering and maintaining the data needed, and completing and reviewing the collection of information. Send comments regarding this burden estimate or any other aspect of this collection of information, including suggestions for reducing this burden, to Washington headquarters Services, Directorate for Information Operations and Reports, 1215 Jefferson Davis Highway, Suite 1204, Arlington, VA 22202-4302, and to the Office of Management and Budget, Paperwork Reduction Project (0704-0188) Washington DC 20503.			
1. AGENCY USE ONLY ***(Leave blank)***	**2. REPORT DATE** September 2005	**3. REPORT TYPE AND DATES COVERED** Master's Thesis	
4. TITLE AND SUBTITLE: Thermomechanical Behavior of Monolithic Sn-Ag-Cu Solder and Copper Fiber Reinforced Solders			**5. FUNDING NUMBERS**
6. AUTHOR(S) Rolando reuse			
7. PERFORMING ORGANIZATION NAME(S) AND ADDRESS(ES) Naval Postgraduate School Monterey, CA 93943-5000			**8. PERFORMING ORGANIZATION REPORT NUMBER**
9. SPONSORING /MONITORING AGENCY NAME(S) AND ADDRESS(ES) N/A			**10. SPONSORING/MONITORING AGENCY REPORT NUMBER**
11. SUPPLEMENTARY NOTES The views expressed in this thesis are those of the author and do not reflect the official policy or position of the Department of Defense or the U.S. Government.			
12a. DISTRIBUTION / AVAILABILITY STATEMENT Approved for public release, distribution is unlimited.			**12b. DISTRIBUTION CODE** A

13. ABSTRACT (maximum 200 words)

Solder joints provide both electrical and mechanical interconnections between a silicon chip and the packaging substrate in an electronic application. The thermomechanical cycling in the solder causes numerous reliability challenges, mostly because of the mismatch of the coefficient of thermal expansion between the silicon chip and the substrate. The actual transition to lead-free solders and the trend towards hotter-running, miniaturized and higher current density chips aggravate this situation. Therefore, improved solder joints, with higher resistance to creep and low cycle fatigue, are necessary for future generations of microelectronics. This study focuses on a thermomechanical behavior comparison between monolithic Sn-Ag-Cu, copper fiber and copper ribbon cylindrical reinforced solders. The composite solders were found to reduce the inelastic strain range of the joint relative to monolithic solder, but at the expense of increased stress range.

14. SUBJECT TERMS Thermomechanical Cycling, Low-Cycle Fatigue, Copper Reinforced Solder, Nickel-Titanium Reinforced Solder.			**15. NUMBER OF PAGES** 71
			16. PRICE CODE
17. SECURITY CLASSIFICATION OF REPORT Unclassified	**18. SECURITY CLASSIFICATION OF THIS PAGE** Unclassified	**19. SECURITY CLASSIFICATION OF ABSTRACT** Unclassified	**20. LIMITATION OF ABSTRACT** UL

NSN 7540-01-280-5500 Standard Form 298 (Rev. 2-89)
Prescribed by ANSI Std. 239-18

THIS PAGE INTENTIONALLY LEFT BLANK

Approved for public release, distribution is unlimited.

THERMOMECHANICAL BEHAVIOR OF MONOLITHIC SN-AG-CU SOLDER AND COPPER FIBER REINFORCED SOLDERS

Rolando Reuse
Lieutenant, Chilean Navy
B.S., Chilean Naval Polytechnical Academy, 1996

Submitted in partial fulfillment of the
requirements for the degree of

MASTER OF SCIENCE IN MECHANICAL ENGINEERING

from the

NAVAL POSTGRADUATE SCHOOL
September 2005

Author: Rolando Reuse

Approved by: Indranath Dutta
Thesis Advisor

Anthony Healey
Chairman, Department of Mechanical and
Astronautical Engineering

THIS PAGE INTENTIONALLY LEFT BLANK

ABSTRACT

Solder joints provide both electrical and mechanical interconnections between a silicon chip and the packaging substrate in an electronic application. The thermomechanical cycling in the solder causes numerous reliability challenges, mostly because of the mismatch of the coefficient of thermal expansion between the silicon chip and the substrate. The actual transition to lead-free solders and the trend towards hotter-running, miniaturized and higher current density chips aggravate this situation. Therefore, improved solder joints, with higher resistance to creep and low cycle fatigue, are necessary for future generations of microelectronics. This study focuses on a thermomechanical behavior comparison between monolithic Sn-Ag-Cu, copper fiber and copper ribbon cylindrical reinforced solders. The composite solders were found to reduce the inelastic strain range of the joint relative to monolithic solder, but at the expense of increased stress range.

THIS PAGE INTENTIONALLY LEFT BLANK

TABLE OF CONTENTS

THIS PAGE INTENTIONALLY LEFT BLANK

LIST OF FIGURES

THIS PAGE INTENTIONALLY LEFT BLANK

LIST OF TABLES

THIS PAGE INTENTIONALLY LEFT BLANK

ACKNOWLEDGMENTS

I wish to acknowledge help, guidance and encouragement provided by Dr. Indranath Dutta during the evolution of this research project. This work was also supported by the Army Research Office.

I would also like to thank my wife Carolina and daughters Marianne, Andrea and Stephanie, who patiently understood all the time and weekends spent at school. They were very important to my achieving this monumental goal.

THIS PAGE INTENTIONALLY LEFT BLANK

I. INTRODUCTION

Surface mount technology (SMT) is used to make the attachment of electronic devices, such as integrated circuit chips or resistors, which are surface-attached to a printed circuit board (PCB), without the need for through holes. This technology was widely developed in the 1980s, mainly due to the introduction of personal computers and the need for greater density of electrical connections per integrated circuit (IC) chip [1]. The most common method for IC packaging is the use of a ball-grid array (BGA), illustrated in Figure 1. This array provides electrical and mechanical connections between the chip and the PCB, allowing for a significantly higher density of electrical connection leads per chip. In actual flip-chip application, the BGA solder balls may initially be placed on the PCB and the chip placed over the BGA. The system then passes through a furnace that melts the solder and provides a permanent connection between the BGA and the PCB [2]. The composition of the solder alloy and the temperature are chosen carefully so that the solder does not completely melt, but stays semi-liquid, which allows for the assembly to maintain the correct separation distance and each ball to stay separate from its neighbors.

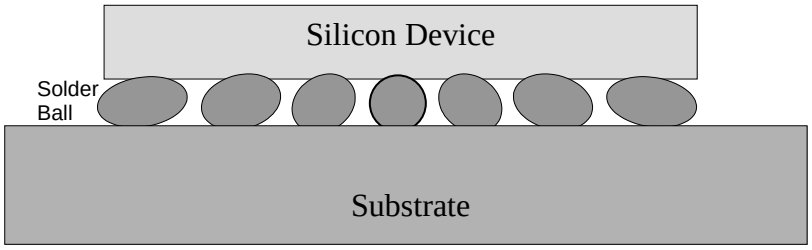

Figure 1. Cross Section of Electronics Package Assembly.

The reliability of solders is critical to electronic packaging since they provide both electrical and mechanical connections between different levels of the package. One of the problems faced is the thermomechanical fatigue (TMF) failure of solders arising from a combination of temperature fluctuations and the Coefficient of Thermal Expansion (CTE) mismatch between the chip and the PCB joined by solders [3]. The CTE of the silicon (Si) chip is significantly less than that of the PCB, and this induces cyclic

mechanical shear strains on the solder under thermal cycling conditions. Due to this CTE mismatch, the solder balls are subjected to severe thermo-mechanical cycling (TMC) conditions as the chip is periodically powered on and off, which can potentially result in solder failure. The periodic cycling results in TMC throughout the integrated component, subjecting even the connecting solder balls to severe creep and low-cycle fatigue (LCF) conditions and over time, certain failure [4, 5].

The situation will become more complex as device miniaturization, lighter weight, higher current density and multifunction result in greater heat generation and possibly higher temperature ranges, coupled with the need to further reduce of size of the solder balls [3, 6, 7]. The deformation behavior is further complicated by microstructural evolution, since solders generally operate at a high homologous temperature (T/Tmelt near 0.8 and higher). Thermally induced grain growth, mechanical stress-induced grain growth and recrystallization has been observed in the high stress regions (Si/solder interface), which has been shown to be prone to fatigue cracking [8, 9, 10, 11]. In addition, the formation and growth of intermetalic compounds (IMC) between solders and substrate have a detrimental effect on the reliability of the solders.

In the past, Sn-Pb solders have been widely used in the electronic packaging industry for their low cost, ease of manufacturability and the good wetting behavior on the Cu, Ni, Ag and Au substrates, which made Pb solders the best candidate for electronics. However, health and environmental concerns have resulted in legislation that has tended to prohibit lead-containing products and placed pressure on the electronic industry [12, 13]. Among these lead-free solders, the Sn-Ag and Sn-Ag-Cu solders are the promising candidates to replace Sn-Pb solders for mainly two reasons. First, it does not contain Pb. Second, the material may be used at a higher service temperature because of its higher melting point compared to Sn-Pb solders (221 oC instead of 183 oC).

Because the trend in the electronic industry is the miniaturization of components, solders with better performance and higher reliability are needed. Mechanical strains induce microstructural coarsening, which reduces the strength of the solder and aids the localization of shear strain near the Si chip surface, and these higher strain ranges lead to TMF failure of the solder. Due to this, there is a need to reduce the strain range near the

Si chip. In recent years, in order to improve the mechanical properties of the Sn-Ag solder and the reliability of the solder joint, a composite solder approach has been adopted [14]. In this composite solder approach, second phase reinforcements are introduced intrinsically (in situ) or extrinsically (dispersion strengthened) into the eutectic Sn-Ag or Sn-Ag-Cu matrix to enhance the following properties of the solder: mechanical strength, creep resistance, TMF resistance and subsequently, solder joint reliability [14, 15]. These reinforcements can be metallic or intermetalic particles like Cu, Cu3Sn, Ag, and Ni. Studies have shown that the composite approach is effective in improving the strength and creep resistance of solders by retarding grain-boundary sliding, impeding grain growth, and redistributing stresses uniformly [16]. However, this approach can only provide some improvements in stress controlled fatigue life, as in TMF life under strain-controlled conditions, which is a primary deformation mode in electronic packaging, the standard composite strengthening approach has not exhibited needed improvements [17, 18,].

One way to achieve better life performance in solders is by producing ‘smart’ or ‘adaptive’ solders that can reduce strain concentrations within joints. This approach consists of the incorporation of soft martensitic shape memory alloy (SMA) particles into the solder. The SMA needs to have similar yield strength as the solder so that at the beginning of the TMC, the soft martensitic SMA will deform with the solder under thermal-induced shear stress. Once the temperature is above the austenitic transformation temperature (As), the SMA particles will transform from martensite into austenite and reverse to the unstrained shape, which will lead to an increase of SMA stiffness. This will reversely deform the SMA particles and alleviate the strain concentration within the regions of interest within the solder ball, which will consequently improve the solder reliability. The problem with this approach is that there are limited successes to fabricate a solder with these characteristics, mainly due to wettability problems of the SMA particles in the solder matrix [19].

THIS PAGE INTENTIONALLY LEFT BLANK

II. BACKGROUND

A. ELECTRONIC SOLDERS

1. Solders in Electronics

Lead-containing solder balls have generally been employed in the electronic industry for many years. However, because of environmental concerns, the industry is gradually switching to lead-free solders. In Europe and Japan, lead-free solders have been mandated to replace the lead-containing solders by the end of this year, and the U.S. microelectronic industry is going to follow the same tendency. Consequently, there is a need for a comprehensive understanding of the properties and performances of lead-free solders in an electronic package to reach successful applications in the electronic industry.

The most common method of electrical and mechanical connectivity between a silicon chip and PCB structure has been solders. The current package architectures require that solders not only provide the mechanical and electrical connection, but also provide heat dissipation and structural support during system operation. Solder is the softest material in the structure, and plays a vital role in providing system integrity and necessary circuit connectivity in the current microelectronic packaging industry [20, 21].

Microelectronic solder joints are typically exposed to aggressive TMC and creep during service. To meet the increasing reliability demands of future microelectronics, a critical assessment of the mechanical, creep and fatigue properties of actual solder balls is required to provide valuable operational specifications for design. The reliability is generally believed to be directly related to their creep resistance, creep-fatigue interaction and thermomechanical fatigue strength [22].

2. Microstructure in Sn-Ag and Sn-Ag-Cu Solders

Over the past decade there has been significant interest in eliminating lead in solders because of its hazardous nature to life and environment. Certain lead-free solders such as eutectic Sn-Ag and Sn-Ag-Cu solders have emerged, after extensive considerations, as likely candidates to replace lead-containing solder joints. One of their advantages is that they melt at temperatures near 221 ^{o}C, instead of at 183 ^{o}C like the

eutectic 63Sn-37Pb alloy does. This property has led to higher service temperature applications. Other important properties are strength and ductility. The strength and ductility of a solder joint are very important for in-service applications. Solder joints need to demonstrate a good balance between strength and ductility in order to withstand thermal, mechanical and thermomechanical loading [23].

Severe operational environments require that lead-free solder joints have superior performance and high reliability. Quite often, reliability issues are linked to microstructural evolution of solder joint materials. Microstructural evolution at high temperatures may have detrimental effects on the joint integrity [15].

The microstructure of Pb-Sn solders, typical in electronic joints, consists of equiaxed grains of Pb-rich and Sn-rich phases, both of which coarsen. This only affects the diffusional creep component and has little effect on dislocation creep. The opposite takes place in Sn-Ag and Sn-Ag-Cu solders, with diffusional creep having little impact and dislocation creep dominating, and this is a direct result of the differences in microstructure [24].

Lewis, Allen et al. [25] studied the eutectic structure of Sn-Ag and Sn-Ag-Cu systems and found that it is energetically favorable for a two phase structure whose volume fraction is greater than 0.28 to form as a lamellar structure, yet for lower volume fractions the rod-type morphology has the minimum interfacial energy. An increase in volume fraction for a lamellar structure only increases the relative thickness of one phase in the structure without a change in surface area, while the surface area increases in volume fraction in a rod type structure. Although this approach holds for many systems, if an orientation relationship exists between phases, the critical volume fraction at which the transition between rod-like and lamellar morphologies occurs will shift.

The initial microstructural composition depends on the initial fabrication temperature, cooling rate and volume fraction. It is apparent that the ultimate life of a solder joint will be a result of the initial microstructure and operating environment. These will dictate how the material will evolve and how long the solder joint will last.

Conrad et al. [11] proved that for Pb-Sn solders, fatigue life significantly increased as reflowed size decreased, making development of this fine microstructure during manufacture beneficial to joint life.

Lewis, Allen et al. [25] reach an updated version of the Ag-Cu-Sn phase diagram and phase chemistry data for the primary Ag_3Sn and Cu_6Sn_5 phases found together with the eutectic morphology. Ternary eutectics are mixtures of three phases, and because of that, they must have a larger number of morphological classes than the binary eutectic and can be described as combination of fibrous and lamellar phases. The resultant ternary structure depends on three solid-solid and three solid-liquid-solid interfacial energies and two volume fractions. Figure 2 is a schematic drawn that assumes equal interfacial energy between all three phases. For equal interfacial energies and small volume fraction, a rod-like morphology would be expected for a ternary eutectic, in analogy to the binary case.

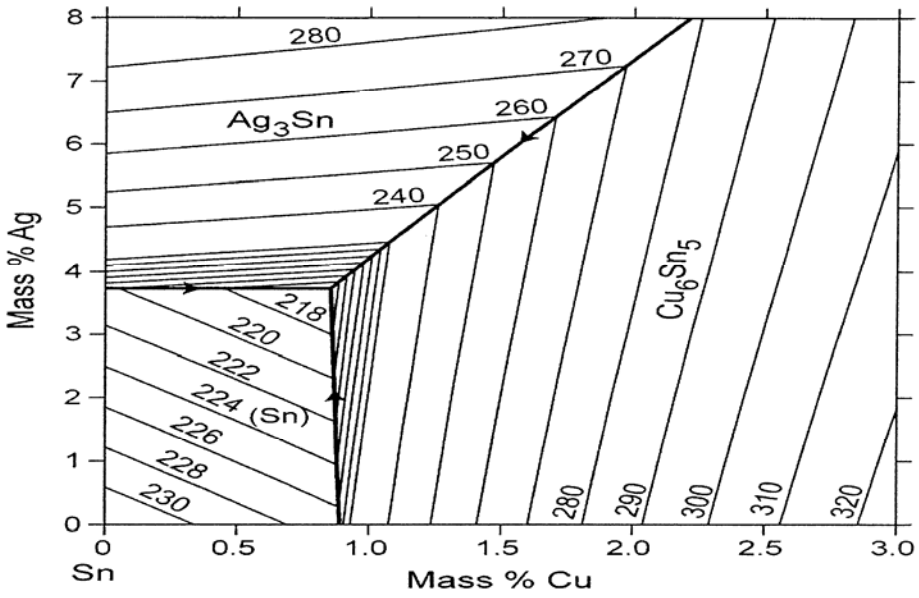

Figure 2. Sn-Ag-Cu Phase Diagram, from reference [22].

During the solidification of Sn-Ag-Cu, phases nucleate heterogeneously in joints and grow, in the form of similarly oriented cells of colonies, towards one another. When two solidifying colonies intersect, a slightly coarsened region of the material forms.

These structures are matastable at room and higher temperatures due to high interfacial energies, which result from a large number of phase boundaries present. This is not the case in solders and the structures formed during solidification, as most alloys are unstable at room temperature. The reduced sizes of SBJ result in structures composed of only a few grains, sizes in which (unlike the bulk) the heating and cooling effects on the microstructure and grain composition are pronounced for even small temperature excursions and that further destabilize the solder material. The effects of temperature fluctuations are the key to the structural properties of the materials involved in solders [26].

In temperatures above 20 ^{0}C, 0.6 T_{melt} for Sn-Ag-Cu solders, diffusion mechanisms dominate at these high homologous temperatures and destabilize microstructures [24, 27]. These temperatures, combined with stresses, produce an increase in coarsening (grain and phase) and microstructural destabilization. Eventually, the grain size in these coarsened regions becomes so large that it can no longer accommodate the imposed strains. Intergranular cracks initiate and propagate, eventually resulting in joint failure. There are more factors that contribute to these coarsening mechanism and effects, but it has been demonstrated that microstructural composition and its temperature dependence are key factors [11, 21, 24, 28].

To prevent grain growth and grain boundary sliding, especially at the elevated homologous operating temperatures and cycling conditions, the fabrication of stable solder phases is necessary. This stability, if generated during fabrication, benefits both creep and fatigue resistance [27].

During TMC, the size of the intermetalic particles increase because of static and dynamic coarsening. Phase coarsening may be greatly accelerated when deformation is superimposed on temperature because of enhanced diffusion caused by the increased vacancy concentration induced through plasticity. The combined effects of temperature excursions and inelastic strains have been shown to directly contribute to the coarsening mechanisms and ultimately the weakening and failure of SBJ [11, 21, 24, 28].

During thermal aging, damage accumulates at cell boundaries parallel to the direction of the imposed strain. Upon heating, the damage of the joint anneals out

through mass diffusion that causes the cell boundaries to coarsen further. Corresponding to this, large inelastic strains are induced within the joint. These large inelastic strains are concentrated in bands running parallel to the solder/bond pad interface, and do not completely relax even during dwell times at the highest temperatures experienced during service because of the constraints present in the joint. The regions near the sidewalls of the joints, where the cumulative strain is the least, retain the original microstructural scale and size after thermal cycling, whereas the regions near the bond pads, where the strains are high, show the maximum amount of coarsening. Microstructure within the joint is homogenous, with the extent of coarsening appearing to increase with increasing cumulative strain [11, 28].

3. Mechanical Behavior of Solders

In surface mount technology, micro miniature surface-mounted components are soldered directly onto the surface of a PCB. In this assembly, the solder serves both as an electrical connection and mechanical member. Due to the mismatch in CTE between the SMC and the PCB, thermo mechanical fatigue is believed to be the major failure mode in solder joints when the individual parts are subjected to temperature fluctuations. The latter is a result of either power switching or the external environment. The solder joints experience a combination of creep and cyclic shear deformation during thermal cycling. Since they operate at high homologous temperatures (T/T_{melt} approaching 0.8), creep is believed to dominate the deformation processes. The inelastic deformation causes the accumulation of damage in solder joints and eventually leads to TMF failure [1, 14, 29, 30, 31].

The two common creep tests that are performed on solder joints in various studies are stress rupture and stress relaxation tests. In the stress rupture test, the test load is held constant while the strain is monitored as a function of time. In the stress relaxation test, the specimen is initially loaded to a specific stress and then held at the constant displacement. Relaxation of load as a function of time is then monitored. The asymptotic value over a long time provides the internal stress in the material. Data from both of these tests are important to estimate the strain ranges experienced by a solder ball under thermal cycling conditions. By investigating the steady state creep rate and the activation energy, one can obtain insight on the creep mechanism of solders [30, 32, 33].

In creep studies, creep deformation behavior is also of interest, since the strain for the onset of tertiary creep may be considered as a failure criterion for evaluating solder reliability. Using a novel mapping technique developed by Lucas et al. [31], both the global and the local creep shear strain were captured and analyzed. The results showed that the creep deformation in eutectic Sn-Ag and Sn-Ag-Cu solder joints was far from uniform along the joint thickness. Enhanced creep strain occurred on both sides of the solder joint, while the creep strain in the mid-region was much lower. One reason may be a smaller cross-sectional area of the solder near the substrate (arising from the solder ball geometry), which must necessarily carry a larger shear stress compared to the cross section midway between the chip and the PCB. This stress difference would lead to larger inelastic creep strain accumulation near the substrate interface, compared to a location further away from the substrate. The larger strain near the interface is consistent with the observed failure mechanism of solder joints subjected to thermal cycling. It was found that cracks initiated and propagated along the IMC/solder interface, or through the solder lying very close to the interface, and the IMC formed due to reaction between solder and the Cu connection strips [3, 34]. The shear strain in the length direction of solder joints was also found to be non-uniform, which could be evidenced by the heterogeneously coarsened region in the Sn-Pb joint after thermal cycling [6]. The most extensive coarsening was found to occur in regions where the highest shear strains were imposed, typically at the end of the joint. Indeed, strain localization in solder joints is a major cause of failure because most of the strain is borne only by a small volume of the solder, which is softened by microstructural coarsening [32]. Studies by Hacke et al. [9] showed that the microstructure of Pb-Sn coarsened in both isothermal annealing and TMC. Furthermore, the coarsening rate under thermal cycling conditions was appreciably greater than isothermal conditions. Figure 3 illustrates microstructural coarsening associated with thermal cycling. The figure shows that the magnitude of coarsening, visible through larger black dots, was significantly greater near the interface, which carries a larger amount of inelastic strain. Clearly, the scale of the intermetalic particles (Cu_6Sn_5 and Ag_3Sn) increases with the severity of the TMC condition. In b, before the joint fails, it is clear that the coarsening is greater in regions of strain localization near the top and bottom interfaces.

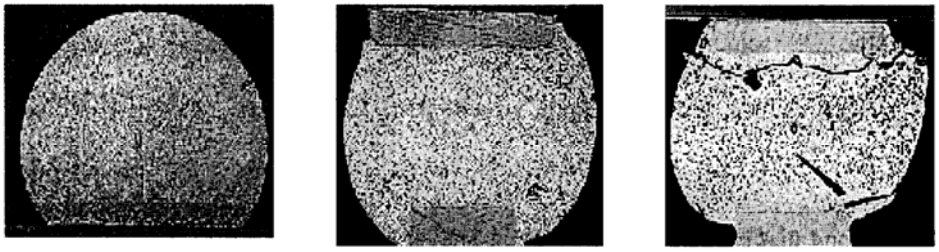

Figure 3. Flip chip joint of Sn-Ag-Cu solder after (a) 2 re-flows, (b) and (c) 2 re-flows followed by 150 thermomechanical cycles between -55 ^{o}C and 125 ^{o}C, with (c) being subjected to twice the shear strain range as (b), from reference [4].

B. REINFORCED SOLDERS

In microelectronic packages, copper substrates are commonly used and Cu_6Sn_5 phase particles are generated near the solder substrate interface. Whether added intentionally or as a result of a reaction near material interfaces, these particles have shown little growth when placed under similar conditions. This is especially important when considering the need for a micro-structural constituent that can remain relatively stable at elevated homologous temperatures for extended times. Stable phases are necessary to prevent grain growth and grain boundary sliding, and this stability should benefit both creep and fatigue resistance [35].

Several approaches have been reported to improve Sn-based solder properties, such as mechanical strength, creep resistance, thermomechanical fatigue resistance and solder joint reliability. The composite approach is one of the potential methodologies to improve the properties of lead-free solder joints. The mechanical behavior of the composite solder joint depends on the reinforcing phases present. Such reinforcements can be introduced by in situ methods or by mechanical means. Compatible inter-metallic compounds (IMC) can be produced by converting metallic particles during reflow. Mechanical properties of the composite solder joint will also depend on the type of IMC and its morphological features.

Studies dealing with the formation of an IMC around intentionally incorporated Cu, Ag, and Ni particles within the eutectic Sn-Pb and Sn-Ag matrix have shown that various morphological features can result as a consequence of the reflow condition. For example, the IMCs formed around Ag particles neither change significantly in volume nor change their morphology under different reflow conditions. Copper particles in reinforced composite solders show significant growth of IMC layers that can completely consume Cu particles. However, this composite also does not exhibit significant changes in IMC morphology as a consequence of reflow profiles. The IMC formed around the Ni particles in the Sn-Ag-based solder matrix exhibits significantly different morphological features based on reflow profiles and the presence of Cu [35].

Published literature indicate that the composite approach is effective in improving the strength and creep resistance of solders by retarding grain-boundary sliding, impeding grain growth, and redistributing stress uniformly [16]. Betrabet et al. [36] showed that the initial as-cast grain size of the dispersion-strengthened (DS) solder was finer than that of the regular one. In addition, after exposure to elevated temperatures, the grain size of the DS solder remained finer than that of the regular solder, indicating that the dispersoids had retarded grain growth. This resistance to grain coarsening may be ascribed to interphase-boundary pinning by the dispersoids. McCormack et al. [37] found that magnetic dispersion processing a Sn-2.5% Fe composite solder and a Bi-43% Sn + Fe 2.5% composite solder exhibited twenty and five times improvement, respectively, in creep resistance at 100 ^{0}C. Guo et al. [15] revealed that the creep resistance in the composite solder, reinforced with Cu particles, was significantly improved. In contrast, although the deformation of an Ag particle-reinforced composite solder was highly uniform throughout the thickness, the improvement in creep properties was far less. Choi et al. [38] performed constant-load creep tests on the eutectic Sn-Ag solder and its in situ composite solders reinforced with 20 vol.% of Cu_6Sn_5, Ni_3Sn_4, and $FeSn_2$ intermetalic particles respectively at room temperature, 85 ^{0}C, and 125 ^{0}C. Their results showed that the creep resistance was similar in magnitude for all alloys at elevated temperatures. At room temperature, the $FeSn_2$ composite solder was found to be the most creep-resistant alloy. Studies by McDougall et al. [17] also showed that the composite solder, which consisted of the eutectic Sn-Ag solder with Cu_6Sn_5 intermetalic particles,

exhibited superior room temperature creep resistance compared with the non-reinforced solder. However, the advantage disappeared at elevated temperatures, where the creep resistance of both types of solders was found to be similar. This phenomenon may be attributed to one, or the combination, of the following causes:

- At elevated temperatures, there is rapid relaxation of the matrix stress immediately adjacent to the particles, leading to loss of load carried by the particles. Therefore, the matrix cannot be effectively strengthened by the reinforcements [17].
- Particles formed by the in situ method tend to coarsen by the diffusional processes in a reasonable time [36, 39].

Overall, it appears that a composite approach does provide benefit under creep conditions. While this is encouraging, the results of fatigue cycling are not as promising. Studies with Cu_6Sn_5 and Ni_3Sn_4 dispersions produced in eutectic Pb-Sn (with added Cu or Ni) by rapid solidification showed that the intermetalic reinforcements did enhance the stress-controlled fatigue life under isothermal conditions [18]. However, their studies showed reduced strain-controlled fatigue life, likely because of increased void-nucleation via creep-fatigue interactions. Since the solder is largely under strain-controlled conditions during TMC, the results imply that additional efforts are needed to make a significant impact on the life of solder joints in BGA and flip chip applications.

As seen in the addition of Cu particles, modification of the solder through material addition can yield better properties. To improve the properties of the composite solder requires the stability of a clean metallic state of the surface of the reinforcing particle so that these can be well bonded within the matrix of the resulting composite.

Nickel-Titanium (NiTi) alloys are a binary, equiatomic intermetalic compound. It has a moderate solubility range for excess nickel or titanium and exhibits similar ductility comparable to other metallic alloys. This solubility allows it to be mixed with many other elements, thereby enhancing the overall mechanical properties of the alloy [22, 40].

The problem of stress and strain localization and LCF ideally would be solved through a composite that would mix the best properties of solders (the ductility which

allows strain absorption) with a material which would increase its performance under thermal and stress fluctuations. The need for differing materials to form interfacial bonds and correctly transfer stresses through these interfaces has minimized the use of many potential reinforced candidates. Shape memory alloys have been proposed as one of the possible reinforcement for solders, more specifically NiTi [40, 41]. NiTi-based shape memory alloys can reduce the effects of strain localization within solder joints. One feature of NiTi which has proven to be helpful and actually compensates for some of the micro structural changes within the solder as it is thermally cycled is that the NiTi reinforcements deform in shear concurrently with the solder during part of the thermal cycle. As the NiTi alloy is thermally cycled, it undergoes a martensite to austenite (M-A) transformation, placing the solder matrix next to the reinforcements in reverse shear. This reduces inelastic strain concentration and ultimately improves the joint operating life. Reinforcements by austenitic NiTi have been found to simultaneously enhance the stiffness and ductility of solder [40].

The shape memory effect is created by a diffusionless, reversible transformation from a low temperature martensite to a high temperature austenitic phase. NiTi austenite has a CsCl (B2) structure with lattice parameters a=0.412 nm, b=0.2889 nm, c=0.4622 nm and x=96.8. The martensite structure allows for the presence of many twin variants, which can all be converted into one primary variant to produce large plastic deformation [40, 41].

The martensite phase of the alloy is characterized by low energy along the glissile interfaces, which can be driven by small temperature or stress changes in the alloy. A thermal martensite has a herringbone structure that consists of twin related, self-accommodating variants that cause elimination by other variants during shape change. These self-accommodating variants allow for easy deformation to several percents of strain at low applied stress. The austenite phase of the alloy is characterized by higher energy and upon reaching a determined higher thermal activation will return the structure back to the martensite phase. Most importantly, the austenite phase has only one possible orientation, and therefore when heated, the deformed martensite phase must revert to the memorized austenite configuration and return to its original shape [40]. Numerous alloys possess these qualities, but the commercial availability of many is limited. Only those

which yield significant strain recovery (7 to 8%) at a reasonable cost are considered and pursued.

C. OBJECTIVE OF THE THESIS

The objective of this thesis is to evaluate and compare the thermomechanical response of a cylindrical Sn-Ag-Cu monolithic solder, a cylindrical Sn-Ag-Cu solder reinforced with a single Cu fiber and a cylindrical Sn-Ag-Cu solder reinforced with a single Cu ribbon, to demonstrate concept viability of an improved solder system under TMF cycling conditions.

THIS PAGE INTENTIONALLY LEFT BLANK

III. EXPERIMENTAL PROCEDURE

A. SAMPLE PREPARATION

1. Solder Flux

The first step in the development process of the samples is the production of the solder flux. This solder flux is particular to the production of solder bumps used in microelectronics. This flux was fabricated using a method similar to that developed by T. Fang et al [22, 42]. The flux uses a low reflow temperature and is self-cleaning.

The solder flux is composed of 2.5 parts in weight of polyethylene glycol (PEG, Aldrich # 20, 243-6) a white waxy solid, 1.6 parts of Adipic acid (Aldrich # A2635-7) a white solid powder, and 5.9 parts of polypropylene glycol, (PPG, Aldrich # 20, 235-5) a transparent glycerin-like liquid. The constituents were placed in a suitable-sized glass laboratory beaker, and the mixture was stirred with a Stir-Pak laboratory mixer model No. 4554-12 and associated impeller type mixing blade, while being heated with a Thermolyne model HP-A1915B hot plate, until a temperature of 200 ^{o}C was reached. The initial stirring speed was between 50 to 100 RPM to provide thorough mixing of all ingredients. The temperature of the solution during stirring was carefully monitored and when the temperature reached approximately 150 ^{o}C, the mixture started smoking. When the mixture reached 200 ^{o}C, the stirring rate was increased to 250 to 300 RPM and this speed was maintained until the mixture turned to one single phase with no particulates.

Once a single-phase solution was achieved, the mixture was removed from the hot plate heating surface and air cooled to approximately 120 ^{o}C, while maintaining the stirring of the mixture at 250 to 300 RPM. The mixing was stopped and the beaker was quickly immersed into a water bath in order to rapidly quench the solution, while simultaneously stirring the mixture at 150 RPM. This step breaks down the Adipic acid precipitates into fine 25 micron particulates. Stirring was continued until a solution temperature of 30 ^{o}C was reached. At this stage, the solution was transferred to a sealable container (a suitable lab bottle) and stored at room temperature until ready to use.

2. Monolithic Sample

For ease of handling and to aid in consistency, all soldering of joints was accomplished with disk performs, which were cut from a sheet of 0.3 mm thickness. The sheet consisted of cold rolled bulk Sn-Ag-Cu, followed by punching 3 mm diameter disks. The type of joint tested was the single joint shear (SJS), which does not model any electronics package joint but is used for comparison of materials. For this joint, 99.9% pure copper rods were machined to 5.9 mm diameter by 19 mm length. The rod ends had a recessed cup of 3.175 mm in diameter with a depth of 0.38 mm placed on one rod end. Figure 4 shows nominal Cu rod dimensions for cylindrical samples.

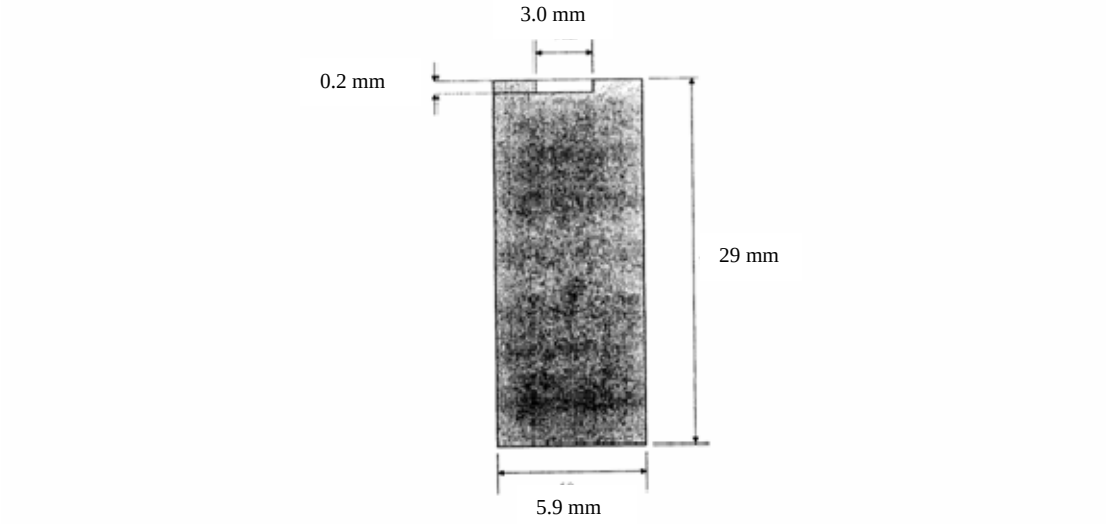

Figure 4. Cylindrical Recessed Cup Type Cu Rod, after reference [20].

A thin film of aluminum was then vapor deposited onto this end surface. Physical Vapor Deposition (PVD) was used to form the metallic thin film on the polished Cu surface. This procedure began by filling two tungsten wire baskets with cleaned, polished and sectioned pieces of Aluminum. The polished Cu rods were attached to a heated sample holder and placed in the PVD vacuum chamber. The PVD chamber was drawn down to a vacuum of $5x10^{-8}$ torr. The Cu temperature was then increased to 300 ^{o}C and held at that temperature for 2 hours. This was to remove any residual surface contamination. The Cu temperature was decreased to 155 ^{o}C. Once the temperature stabilized, vacuum evaporation was initiated. While the substrate was held at 155 ^{o}C, current was applied to the tungsten baskets at 1 Ampere (A) per minute until 30A of

current were achieved. It is important to keep close watch of the amperage applied to the tungsten coils. As the Al chips settle in the basket, the current across the basket can quickly spike to over 50 A. When this happens one must decrease amperage to prevent breaking the tungsten baskets and damaging the current leads that are attached to them. Current was maintained until at least 1μm of Al film was deposited onto the Cu surface. Film thickness level was measured by an ultrasonic film thickness monitor. The probes holding the tungsten baskets were maintained slightly loose. This allowed for heating expansion, which subsequently maximized the life of the tungsten baskets and allowed for high levels of metal deposition. Figure 5 shows the PVD chamber and the vacuum pump.

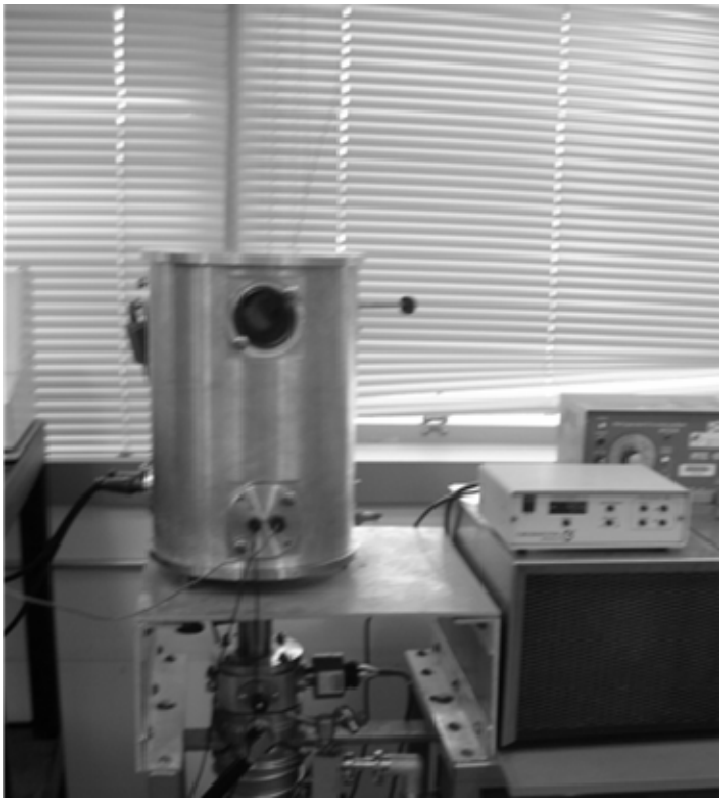

Figure 5. PVD Chamber and Vacuum Pump.

After vapor depositing the aluminum on the copper rod ends, 1000 grit silicon carbide paper was used to remove the aluminum from just inside the recessed cup surface area, while the remaining aluminum was left on the rod ends to serve as a solder mask during joint fabrication. Failure to remove the aluminum from the recessed cup surface

results in poor bonding between the solder discs and the copper surface, or an irregularly shaped joint due to removal of aluminum from the area surrounding the recessed cup. After this procedure, the copper rods were rinsed with acetone, followed by methanol, and then subsequently dried and the recessed cups lightly coated with flux.

Figure 6 is a picture of the furnace that was previously designed to produce SJS samples of the proper dimensions [20]. Previously, samples had been generated inside a closed oven, on a mold with the corresponding dimensions, but many bonding problems between the two copper rods arise. This design allowed for manual manipulation of the sample during its reflow stage, thus giving greater flexibility with the size and shape of the final sample. During solder reflow, the expansion of the solder can be compensated for by adjusting the distance between the two copper rods, thus preventing the solder from overflowing.

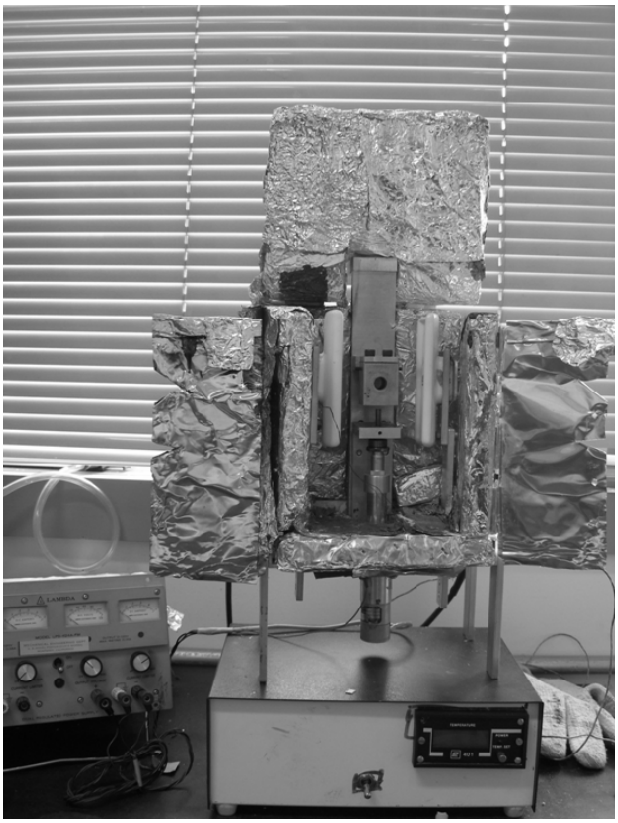

Figure 6. Furnace and Fixture for Manufacture of SJS Type Joint.

The Cu rods described previously were then placed in the removable aluminum crucible fixture mounted in the furnace. The top rod was fixed into position in the crucible using screws, while the bottom rod and the six solder disks (1.8 mm in total) mentioned before were positioned vertically using the anvil of a micrometer. The anvil was adjusted until the three pieces making up the SJS were in contact. At this point, motion of the micrometer controls the position of the lower rod and thus the distance between the two recessed cups. The micrometer is controlled with an electric motor and connected to a DC power supply providing positive control of the joint height during fabrication.

A thermocouple was placed in contact with the upper rod approximately 2-3 mm above the joint and the furnace top, with the front insulation set in place. The 500 W, 120 VAC radiant heaters were then turned on and set to 300 ^{o}C. Once the solder reflowed and expanded, the joint height was adjusted using the micrometer and the electric motor to the desired height (approximately 1.8 mm) and cylindrical shape. The front insulation was opened to a size large enough to see with the unaided eye and the help of a flashlight. This permitted a good control of the entire process and final dimensions.

To generate a sample, solder was reflowed for two minutes at the desired temperature while the final height and cylindrical shape was adjusted manually. At the point of reflow, typically after 10 minutes with the heaters at 300 ^{o}C and the sample temperature at 240 ^{o}C, the joint height was adjusted to 1.8 mm using the electric motor/micrometer. Figure 7 shows nominal solder SJS sample dimensions.

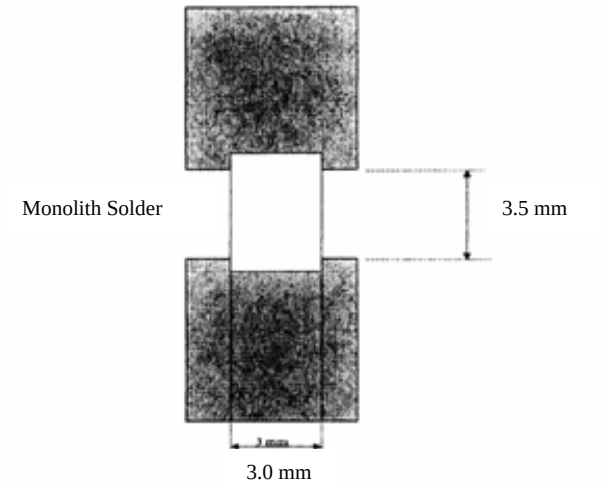

Figure 7. Nominal Recessed Cup Monolith Sample, after reference [20].

In order to cool the joint, the heaters were turned off, front and top insulation was removed, and a fan (placed approximately 20 cm from the crucible) was used to blow cool air directly onto the crucible and joint. The cooling rate was estimated to approximately 20 ^{o}C/min. After cooling the joint to room temperature, the joint was removed from the crucible and was ready for testing.

3. Composite Samples

To fabricate the copper fiber and copper ribbon fiber composite, the solder was heated to 250 ^{o}C, thereby possessing a 29 ^{o}C superheat, and then poured into a graphite mold with a 2 mm diameter hole and a depth of 30 mm. The Cu fiber and Cu ribbon were polished using SiC paper and fluxed with the same flux that was fabricated for the monolith sample. Then, the fibers were dipped into the molten solder and kept in the furnace for 6 minutes at 250 ^{o}C. After cooling the graphite mold to room temperature, the mold was broken and pieces of 2 mm length were cut from the cylindrical composite.

The reinforced cylindrical solder samples were manufactured using the same procedure as that for the cylindrical monolith SJS samples. That is, they were placed in the aluminum crucible while the joint height was adjusted manually to ensure full contact. The resultant Cu single fiber composite had a diameter of 2 mm with a 1 mm diameter fiber at the center. The resultant volume fraction was 18.9% and for the Cu ribbon fiber composite, the volume fraction was 9.8%.

For the NiTi fiber composite solders, the composite was fabricated by dipping the NiTi wire and ribbon into the molten solder multiple times. Initial experiments showed there was a considerable wettability problem between the solder and the NiTi fibers. Simple polishing of the wire using SiC paper was inadequate to remove nascent oxide on the wire, which likely contributed to poor wettability. A good test for this wettability issue was to re-melt the solder after fabrication. Poorly wetted NiTi fibers easily separated out from the composite matrix on re-melting. In the experiments, an Indalloy® Flux #2 was applied onto the surface of the wire before dipping. The wire was submerged for 3 minutes in flux heated to 130 ^{o}C. After reflowing the as-cast solder composite on a hot plate, it was found that the molten solder still adhered to the wire, indicating that the wire was fully wetted by the molten solder. After multiple dips on the molten solder, the mold was placed into the oven for 15 minutes at 250 ^{o}C. The resultant NiTi single fiber composite had a diameter of 2 mm with a 1 mm diameter fiber at the center. The resultant volume fraction was 18.9%. For the NiTi ribbon fiber composite the volume fraction was 9.8%. After the NiTi and Cu composites were ready, they were cut in pieces of 2 mm in length with a diamond saw.

The orientation of the ribbon was one of the key elements to its implementation. That is to say, the ribbon is shaped like a long slender beam. When tested, it was crucial that the shorter axis of the samples lay perpendicular to the direction it was being sheared in. For this reason, as the pieces which compose the sample were being placed in the crucible, a small notch was lodged into both Cu rods to help visually align the sample upon removal from the crucible.

B. APARATUS FOR TESTING

TMC was accomplished by physically cycling a sample from a furnace to a cooler and repeating the cycle. The heating part of the cycle was inside a furnace maintained at 245 ^{o}C by a closed loop controller. At the end of the heating cycle, the sample reached approximately 125 ^{o}C. The cooling system involved air cooling the sample and then applying a small burst of liquid nitrogen to lower the temperature to approximately -20 ^{o}C. Figure 8 shows a typical time versus temperature plot.

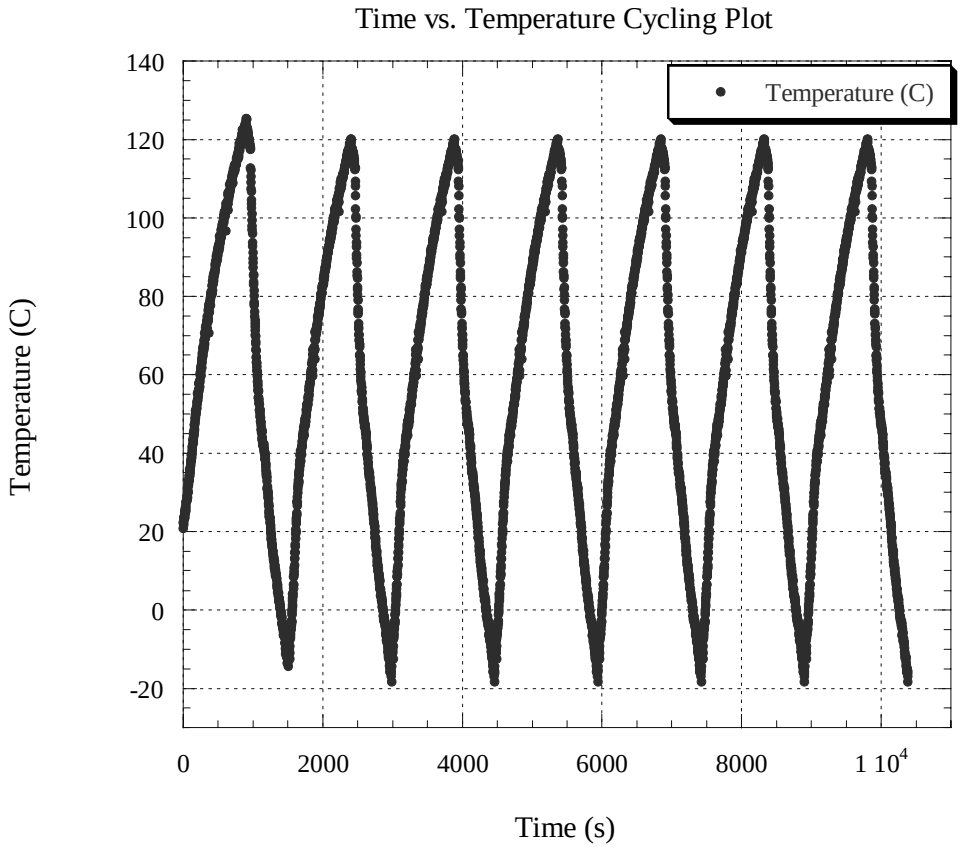

Figure 8. Time vs. Temperature Plot.

A pneumatic ram controlled the movement of the sample from the cooler to the furnace. Air for the ram was directed to the top or bottom of the ram by two solenoid valves connected to a timer, which also controlled the release of liquid nitrogen used in the cooling system. The timer was programmed to cycle the solenoid valves and thus control the thermodynamic profile. Each cycle included 15 minutes inside the furnace and 10 minutes in the cooling section, with the final 9 minutes seeing liquid nitrogen discharged directly onto the sample. Figure 9 shows a picture from the thermal cycling apparatus.

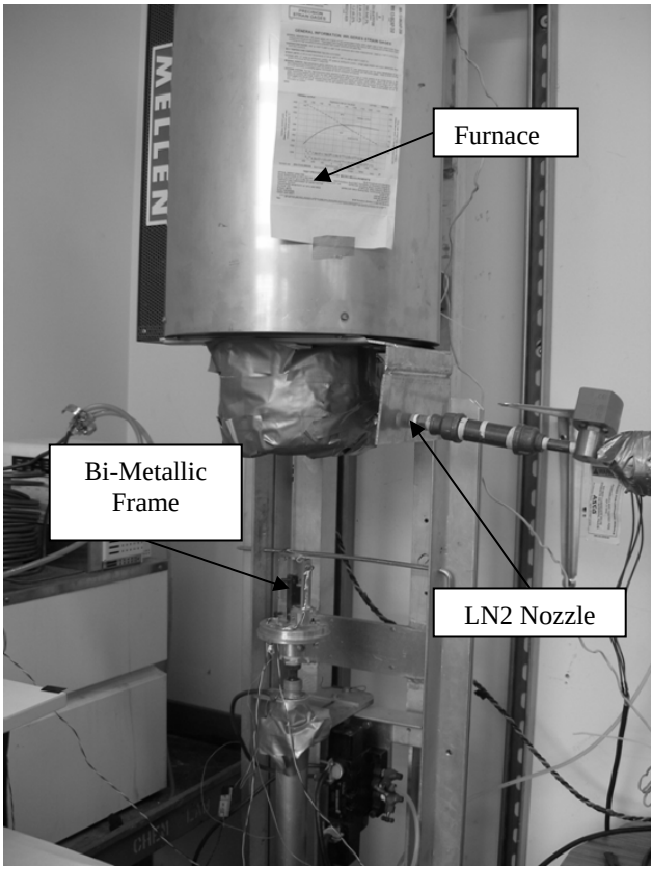

Figure 9. Thermal Cycling Apparatus.

C. THERMAL CYCLING FRAME

The fixture used to stress the SJS joints was derived from the bimetallic frame design of reference [11], and used previously in references [21] and [24]. The frame is illustrated in figure 10 and 11.

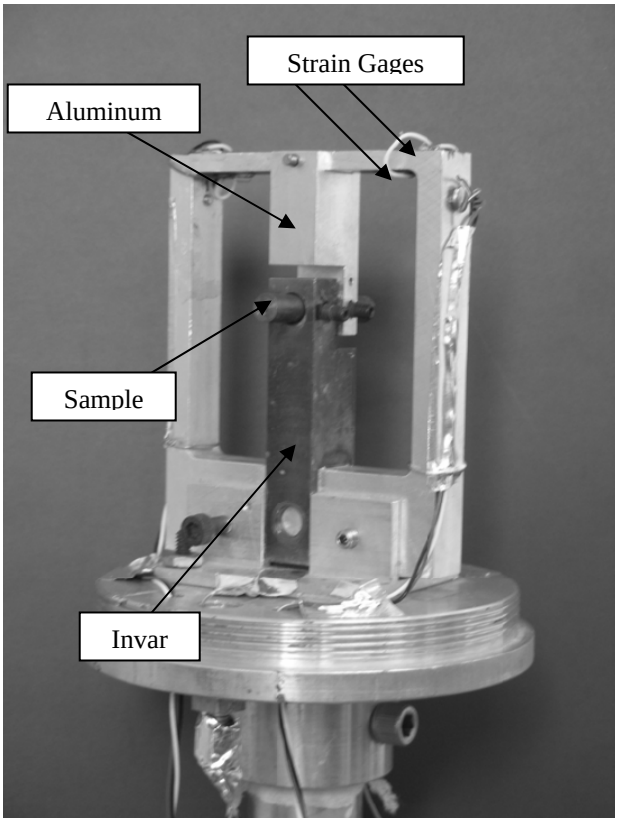

Figure 10. Bi-Metallic Thermal Cycling Frame.

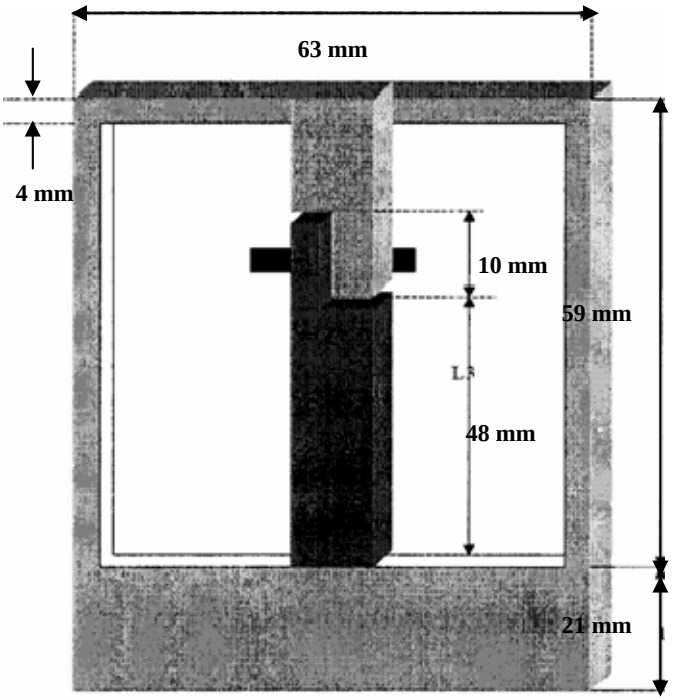

Figure 11. Bi-Metallic Frame Engineering Drawing [20].

In using this frame, the thermal cycle induces a mechanical cycle similar to those encountered by FC electronic devices. As the temperature on the frame is increased in the furnace section, the metals expand based on their CTE, or α, and the formula $\delta = \Delta\alpha * \Delta T * L$ is used, where the temperature is read from a thermocouple placed on the Invar side of the frame. By virtue of the large differences in CTE between the two members of the frame (α_{Al} = 2.28e^{-5} K^{-1} and α_{Inv} = 7.20e^{-7} K^{-1}), the columns expand upwards more than the lower grip, and therefore, a shear is applied to the sample even at small changes in temperature.

If the samples were completely compliant and did not resist shear, the difference in expansion mentioned above would give the displacement of the joint in shear. However, because the samples resist shear, they cause deflection in the upper beam of the frame. This deflection is measured in voltage change by four strain gages placed in pairs on the beam on either side of the upper grip, to compensate for thermal induced strains. They are configured electrically in a Wheatstone bridge. A 10 VDC power supply

provides the excitation voltage, while a signal conditioner amplifies the output 1,000 times. To calculate the deflection in mm, the strain gage voltage is multiplied by a constant of beam stiffness.

The frame was calibrated by placing it in an MTS load unit and imposing known loads to obtain values for millimeters per Volt (mm/V) and Newton per Volt (N/V). Figure 12 and Table 1 show the results of these calibration runs.

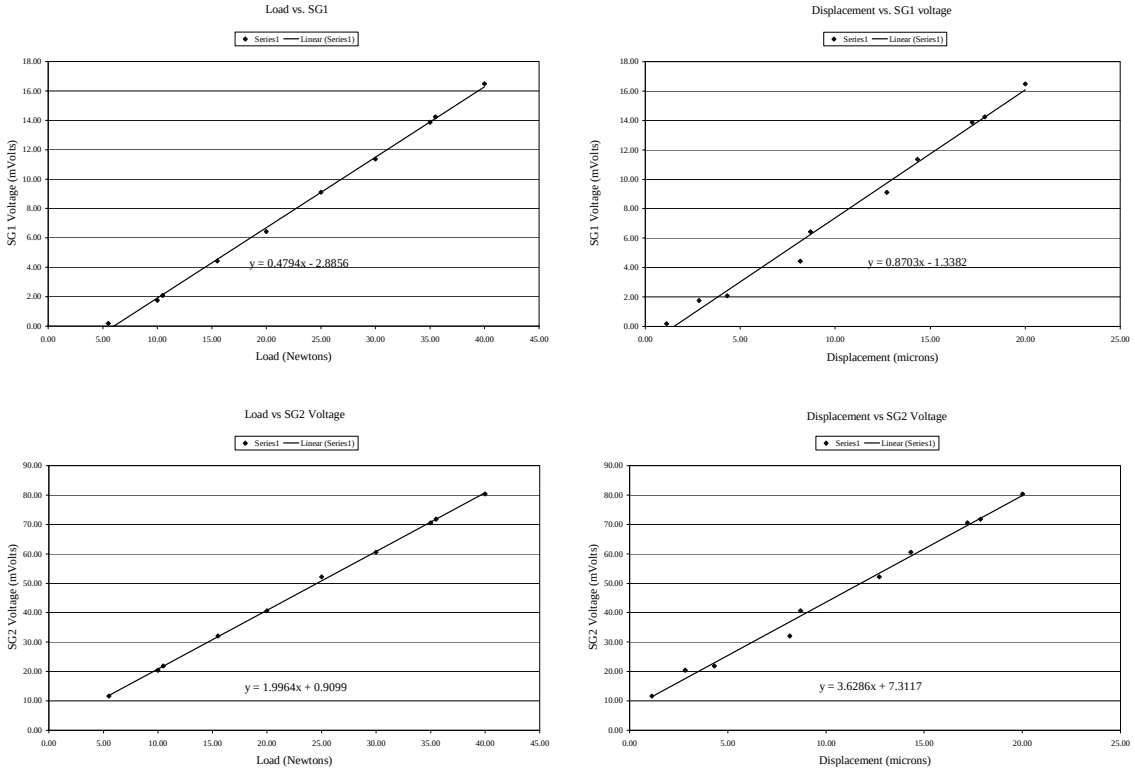

Figure 12. Calibration Results for TMC Frame

STRAIN GAGE	VOLTAGE vs. LOAD	VOLTAGE vs. DISPLACEMENT
SG 1	0.0056497 V/N	9.0992 V/mm
SG 2	0.0059630 V/N	9.6339 V/mm

Table 1. Calibration Results

These values, when in conjunction with a version of the following derivation modified for an Excel spreadsheet, yield stress and strain values on the solder joint. One

starts by seeing that the total shear displacement of the joint without any constraints (or the SJS sample) is equal to the displacement due to CTE mismatch, minus the displacement of the frame. Thus, $\Delta_T = \Delta T \cdot \Delta\alpha \cdot L_{Inv} - \left(\frac{\tau \cdot A}{k}\right)$, or $\Delta_T = \Delta_{Th} - \Delta_{mech}$. If one assumes that with an increase in temperature Δ_T, there is an instantaneous elastic strain (γ_{el}) with no associated instantaneous plastic strain (γ_{pl}), then $\Delta_T \approx \Delta_{el} = \Delta_{Th} - \Delta_{mech}$ and $\frac{\Delta_\tau}{G(T)} \cdot t_{jo\,int} = \Delta T \cdot \Delta\alpha \cdot L_3 - \left(\frac{\tau \cdot A}{k}\right)$. This can be further derived to $\Delta_\tau \cdot \left[\frac{t_{jo\,int}}{G(T)} + \frac{A}{k}\right] = \Delta T \cdot \Delta\alpha \cdot L_3$ or $\Delta_\tau = \frac{\Delta T \cdot \Delta\alpha \cdot L_3}{\left[\frac{t_{jo\,int}}{G(T)} + \frac{A}{k}\right]}$ and with some further simplification $\Delta_\tau = \frac{\Delta T \cdot \Delta\alpha \cdot L_3}{A} \cdot \left[\frac{1}{\frac{t_{jo\,int}}{A \cdot G(T)} + \frac{1}{k}}\right]$. This yields an equation for the change in shear at the solder joint $\Delta_\tau = \frac{k \cdot C \cdot V_{sg}}{A_{jo\,int}}$ (equation a.). To find the change in shear strain for the tests conducted ($\Delta\gamma_{yield}$), an addition of the change in elastic ($\Delta\gamma_{el}$) and plastic ($\Delta\gamma_{pl}$) shear strains is necessary. However, for the purposes of these experiments, the need to generate data for the change in plastic shear strain yields the following: $\Delta\gamma_{test} = \Delta\gamma_{el} + \Delta\gamma_{pl} = \frac{\Delta_\tau}{G(T)} + \Delta\gamma_{pl}$, so finally $\Delta\gamma_{pl} = \Delta\gamma_{test} - \frac{\Delta_\tau}{G(T)}$ (equation b.).

These two equations (labeled a. and b.) allow the tester to use the values for voltage vs. displacement and voltage vs. load to calculate the plastic shear strain and stress at the joint.

D. NITI PARTICLES REINFORCED SAMPLE PREPARATION

1. Nickel Titanium Sizing

Commercially available 1 mm diameter NiTi wire, containing approximately 50.6% Ni and a nominal A_S temperature of 45 ^oC, was selected for use in this study. This wire was chosen for its ready availability. The processing route developed in reference [22] should be independent of the precise composition of the NiTi used, although it is anticipated that, ultimately, a different composition with a higher A_S temperature will

need to be used. The large size of the wire required the development of a methodology for reducing the wire to approximate 15-25 μm-sized particulate for eventual incorporation into the solder.

The commercial NiTi wire (1mm in diameter) was first cold rolled, then hydrogen (H_2) embrittled and finally ground to powders less than 25 microns by mechanical grinding in a mortar. The wire was first annealed at 550 ^oC for 30 minutes so that it could be rolled into a flat strip with a thickness of approximately 0.2 mm.

The solution used for hydrogen embrittlement of NiTi was comprised of normal sulfuric acid and 0.2 grams per liter of Thiourea (Aldrich chemical T33553-500g). In this study, the 1N H_2SO_4 solution was produced using 1 part 95-98% H_2SO_4 (Aldrich chemical 25810-5) diluted by 17 parts of distilled water. A 0.5 mm diameter platinum wire (Aldrich chemical 26722-8) was employed in a coil shape as the anode, and the NiTi wire was used as the cathode in an electrochemical cell, in order to cathodically charge the NITI with H_2. The oxide layers on the annealed NiTi strip surfaces were carefully removed by grinding with 320-grit silicon-carbide sandpaper prior to embrittlement. A current density of 35 mA/cm^2 was adopted to optimize the H_2 evolution rate so that the required amount of hydrogen would diffuse into the NiTi. The NiTi strip had been embrittled for 6-8 hours in the solution.

After the H_2 embrittlement was completed, the brittle NiTi strip was rinsed with distilled water to remove the residual acid solution from its surface, followed by a hot air dry. The embrittled NiTi strip was subsequently ground in a mortar and pestle for approximately 4 hours. After this process, the NiTi powder was sieved to obtain a 25 μm particulate powder. Since a significant amount of cold work had been introduced to the NiTi particles by cold rolling and by mechanical grinding, the fine particles were annealed at 550 ^oC for 30 minutes to recover the high dislocation density in the particles.

IV. RESULTS AND DISCUSSION

A. MICROSTRUCTURES

1. Monolithic Sample

A monolithic sample was mounted and polished, and observed metallographically. Figure 13 shows a monolith sample macrograph.

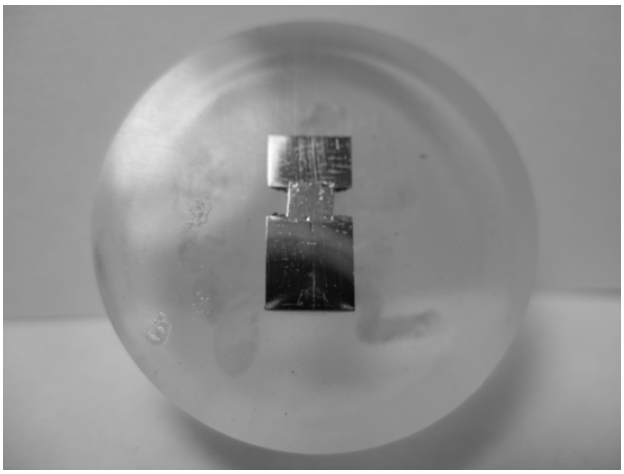

Figure 13. Monolithic Sample Macrograph.

Figure 14 shows the resulting microstructures at 1500x, as observed with a Jenaphot 2000 optical microscope. As observed here, the microstructure consists of a fine dispersion of Ag_3Sn (and some Cu_6Sn_5) precipitants in a β-Sn matrix. Figure 15 shows the same region, but it was taken with a scanning electron microscope (SEM)

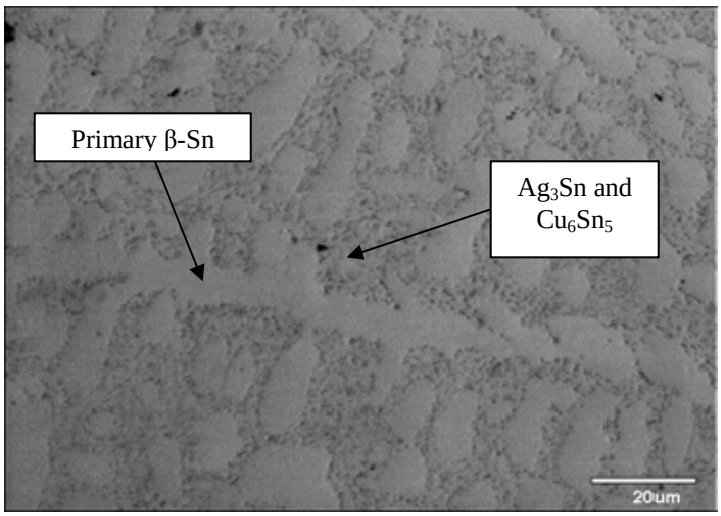

Figure 14. 1500x Optical Microscopy Monolithic Solder.

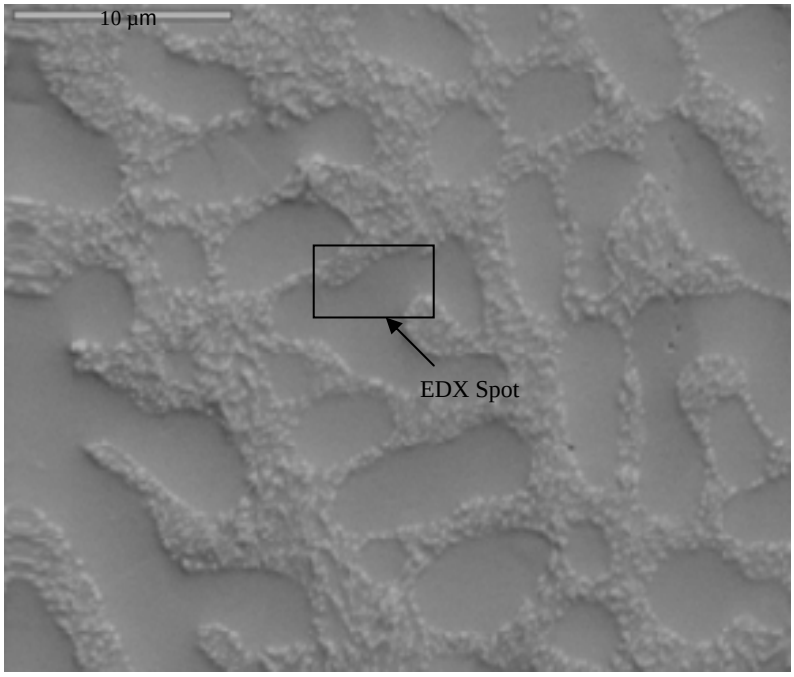

Figure 15. SEM Picture Monolithic Sample.

As can be seen in Figure 16, EDX analysis was used to verify the average Sn-Ag-Cu solder composition. The monolithic solder has the following composition: SnL = 93.91%, AgL = 4.9% and CuK = 1.19%.

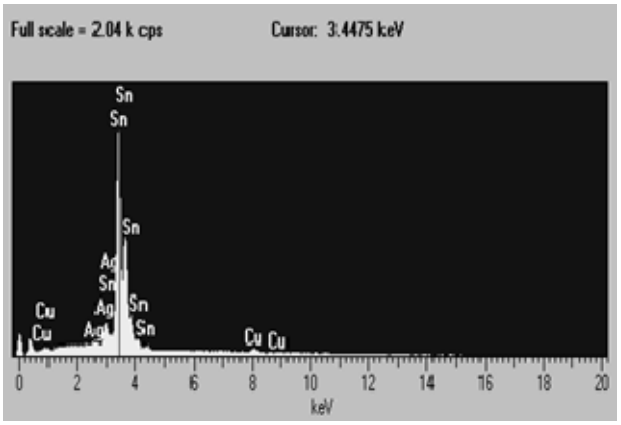

Figure 16. EDX Analysis of Monolith Sample

2. Copper Fiber Sample

A Cu sample was mounted and polished, and observed metallographically. Figure 17 shows a Cu fiber sample macrograph.

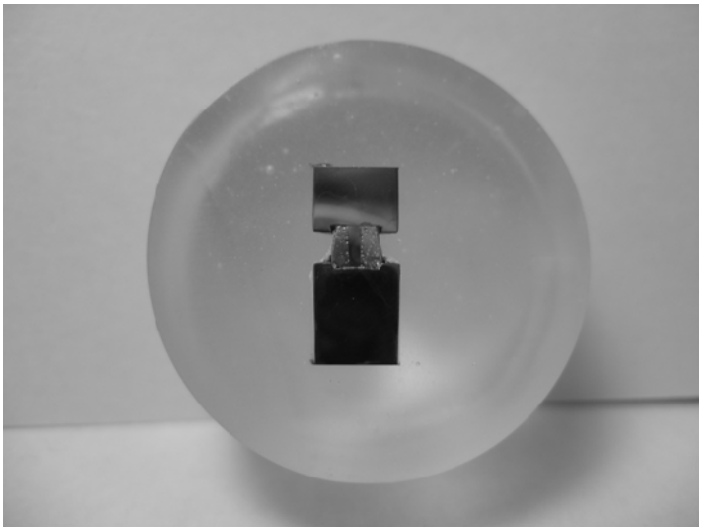

Figure 17. Copper Fiber Sample Macrograph.

Figure 18 shows the microstructure of the copper fiber-matrix interface. It can be seen that this region consists of three colonies: Cu fiber, IMC layer and solder matrix. There are some Cu_6Sn_5 intermetallics in the solder matrix, but in the interface region the Cu content is increased and the Cu_6Sn_5 intermetallics become coarse.

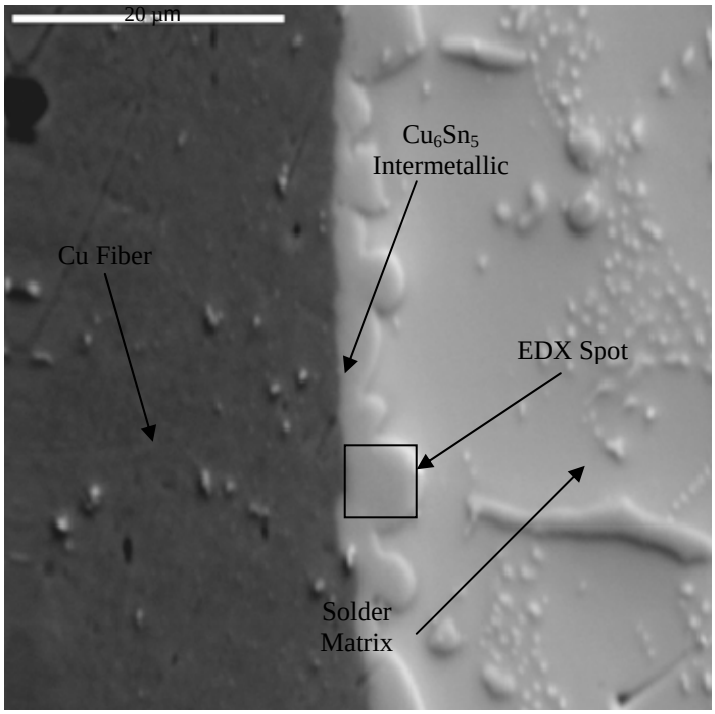

Figure 18. SEM Picture Cu Fiber-Matrix Interface

Figure 19 is a description of how EDX analysis was used to obtain the Cu fiber-matrix interface composition. The spot was located at the interface between the Cu fiber and the solder. The Cu_6Sn_5 intermetallic has the following composition: SnL = 39.6%, CuK = 59.48% and AgL = 0.92%.

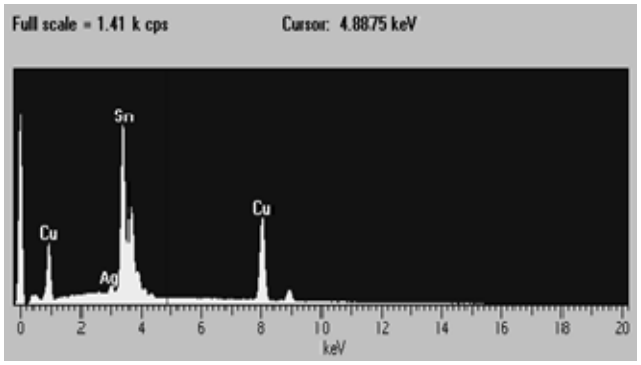

Figure 19. EDX Analysis of Cu Fiber-Matrix Interface

3. Copper Ribbon Sample

A Cu sample was mounted and polished, and observed metallographically. Figure 20 shows a Cu ribbon fiber sample macrograph.

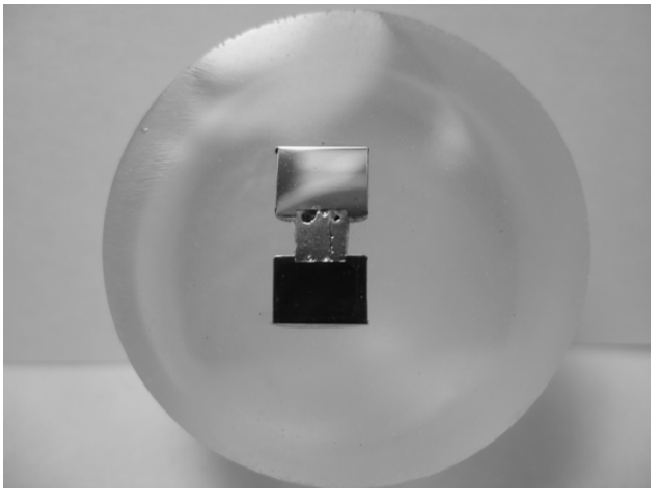

Figure 20. Copper Ribbon Fiber Macrograph.

Figure 21 shows the microstructure of the copper ribbon-matrix interface. It can be seen that this region consists of the same three colonies as the previous sample: Cu fiber, IMC layer and solder matrix. There are some Cu_6Sn_5 intermetallics in the solder

matrix, but in the interface region the Cu content is increased and the Cu_6Sn_5 intermetallics become coarse.

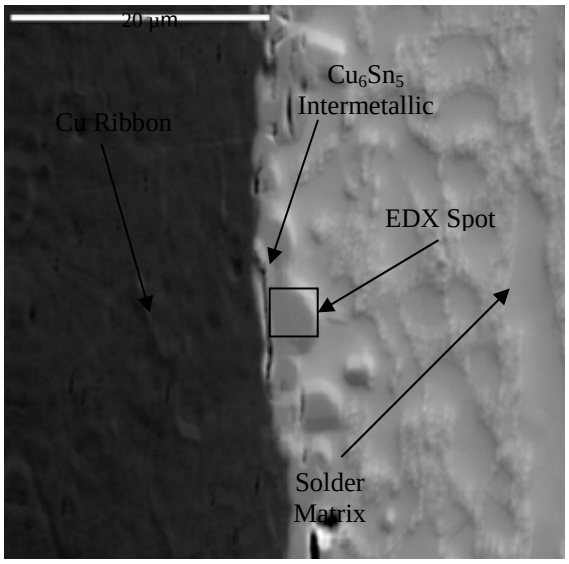

Figure 21. SEM Picture Cu Ribbon-Matrix Interface.

As can be seen in figure 22, EDX analysis was used to obtain the Cu ribbon-matrix interface composition. The spot was located at the interface between the Cu ribbon and the solder. The Cu_6Sn_5 intermetallic has the following composition: SnL = 40.63%, CuK = 58.43% and AgL = 0.94%.

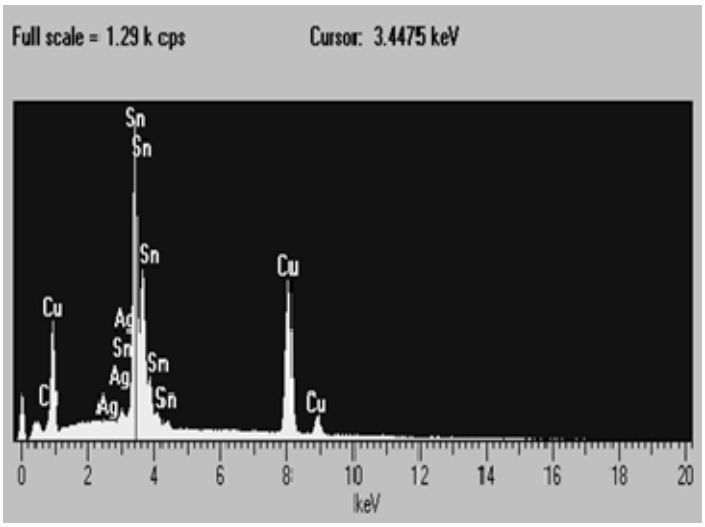

Figure 22. EDX Analysis of Cu Ribbon-Matrix Interface

4. NiTi Fiber and NiTi Ribbon Samples

Evangelos Fountoukidis made the following experiments that can be compared with the previous samples. NiTi fiber and NiTi ribbon fiber samples were mounted and polished, and observed metallographically. Figure 23 shows the macrograph of these samples.

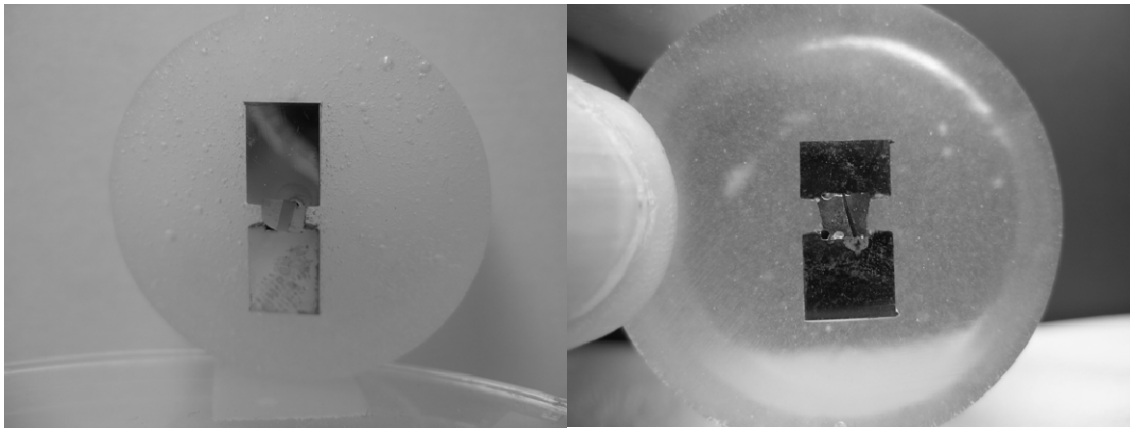

Figure 23. NiTi Fiber and NiTi Ribbon Sample Macrographs.

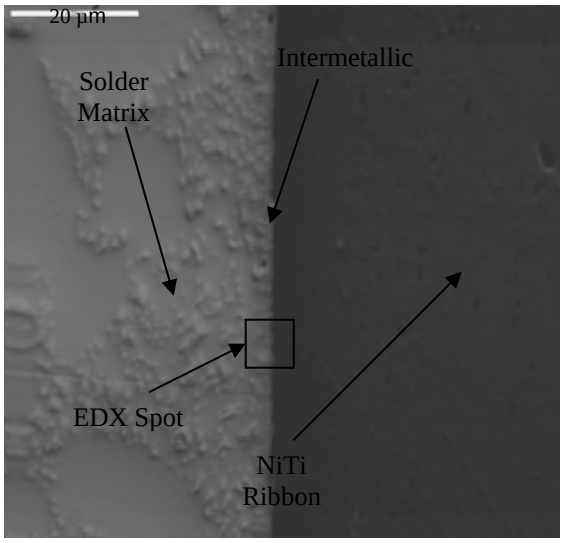

Figure 24. SEM Picture NiTi Tape-Matrix Interface

Figure 25 is an illustration of how EDX analysis was used to obtain the NiTi ribbon-matrix interface composition. The spot was located at the interface between the

NiTi ribbon and the solder. The Cu_6Sn_5 intermetallic has the following composition: Sn = 55.31%, Cu = 6.88%, AgL = 4.37%, Ti = 23.56% and Ni = 9.87%.

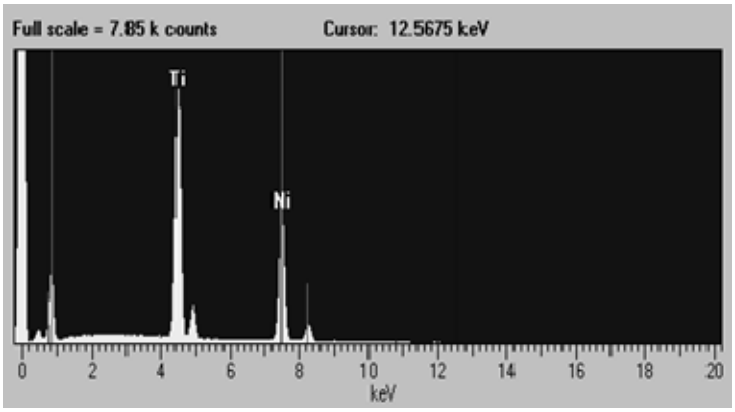

Figure 25. EDX Analysis of NiTi Tape-Matrix Interface

B. THERMOMECHANICAL BEHAVIOR

1. Monolithic Sample

Figure 26 shows an experimentally obtained plot of the average joint shear stress (τ) versus temperature (T) during the 5th cycle for a monolithic solder cylinder. The experimental plots are qualitatively similar to those previously observed for Sn-Ag-Cu solders. The measurement starts with the joint in a stress state at -15 ^{o}C, and the joint stress initially builds up elastically (linearly) until local plasticity and creep mechanisms start operating. Beyond approximately 45 ^{o}C, the plot shows non-linearity with the associated stress relief due to creep. During cooling, the stresses build up again, and below 80 ^{o}C, the joint is subjected to significant inelastic strains with strain localization in shear bands, allowing the stress to return to a small value.

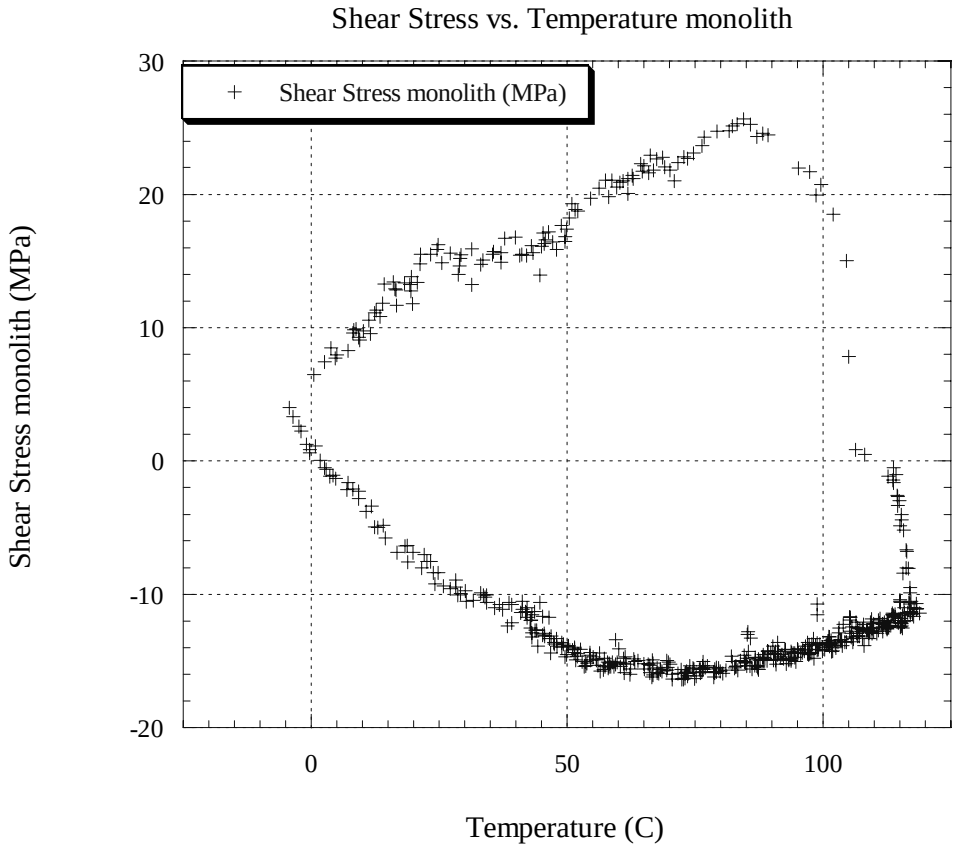

Figure 26. Shear Stress vs. Temperature Plot for Monolithic Sample

Figure 27 is a plot of the average inelastic shear strain ($\gamma_{inelastic}$) versus temperature during the 5th cycle for the same sample. Inelastic strain hysteresis is due to the operation of creep and plastic yielding. While heating, almost no inelastic strain is initially induced as the joint is loaded elastically, following which the high temperature creep/plasticity mechanism becomes operational. The inelastic strains increase rapidly, and during cooling, steadily decrease to values near their original ones.

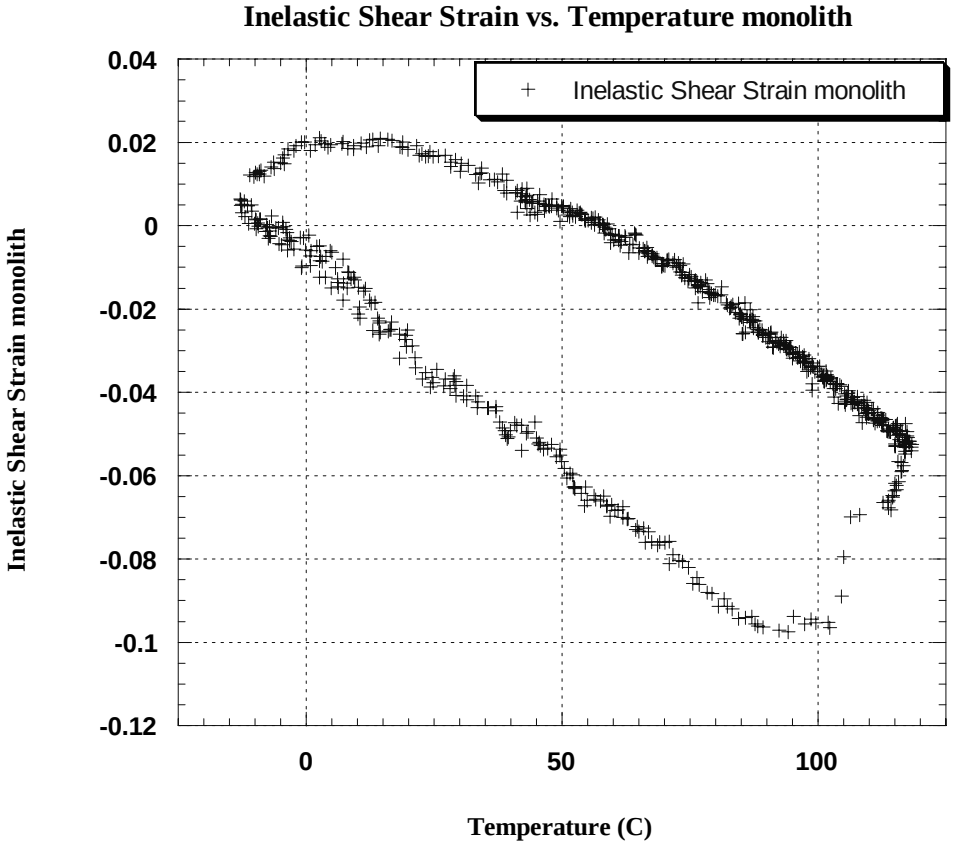

Figure 27. Inelastic Shear Strain vs. Temperature Plot for Monolithic Sample

2. Monolithic vs. Cu Fiber and Cu Ribbon Samples

Figure 28 shows an experimentally obtained plot of the average joint shear stress (τ) versus temperature (T) during the 5th cycle for a monolithic cylinder solder, a Cu fiber reinforced cylinder solder and a Cu ribbon reinforced cylinder solder. The experimental plots are qualitatively similar to those previously observed for these types of solders. The $\Delta\tau$ ($\tau_{max} - \tau_{min}$) for the monolith solder is 40 MPa, 45 MPa for the Cu fiber reinforced solder and 55 MPa for the Cu ribbon reinforced solder. This increase in $\Delta\tau$ was expected because the solders have passive reinforcement. The total increase was 12.5% for the Cu fiber sample and 45% for the Cu ribbon sample. It should be noted here that the copper reinforced solders do not show a reduced creep rate or the reverse creep during heating, which only increases the stiffness of the solder.

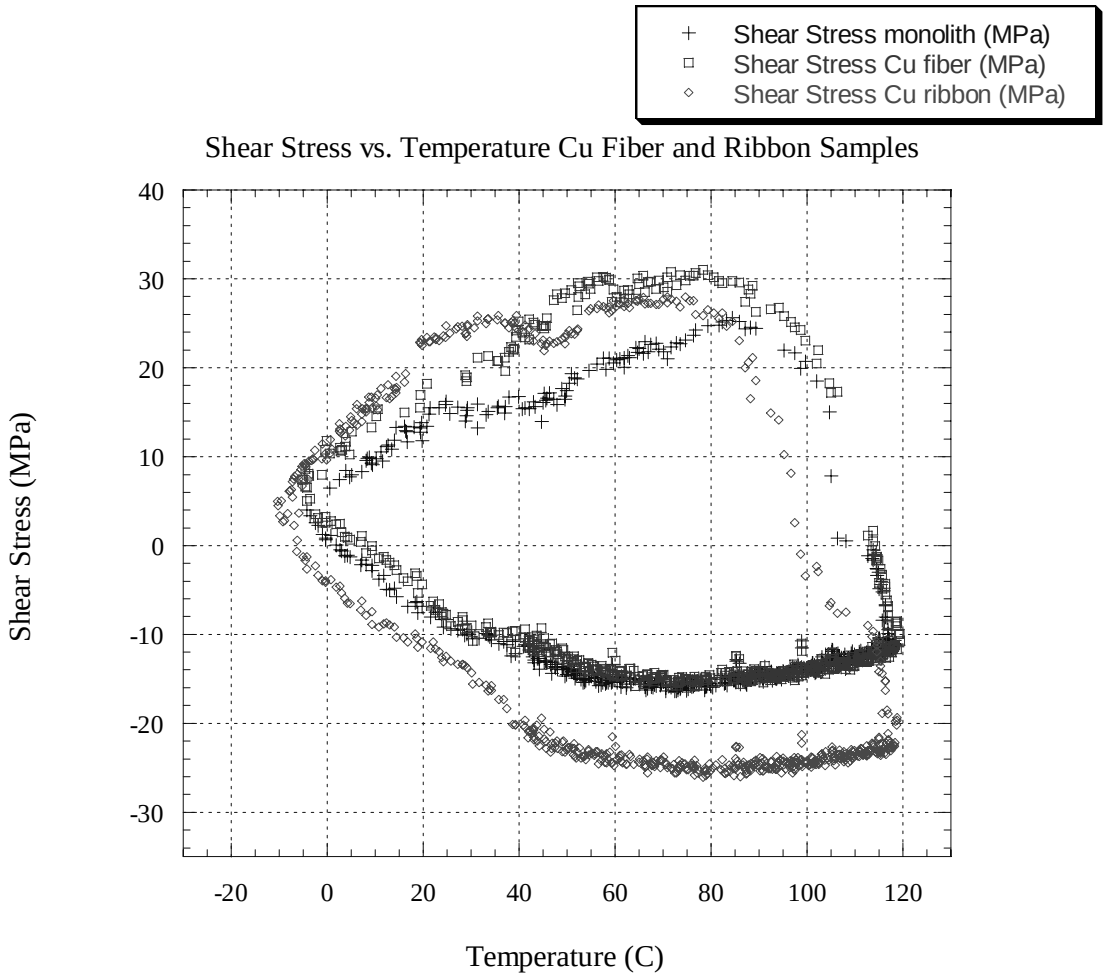

Figure 28. Shear Stress vs. Temperature Plot for Cu Fiber and Cu Ribbon Samples.

Figure 29 is a plot of the average inelastic shear strain ($\gamma_{inelastic}$) versus temperature during the 5th cycle for the same samples. Inelastic strain hysteresis is due to the operation of creep and plastic yielding. The $\Delta\gamma_{inel}$ for the monolith solder is 0.117, 0.095 for the Cu fiber reinforced solder and 0.100 for the Cu ribbon reinforced solder. The total decrease was 18.8% for the Cu fiber sample and 14.5% for the Cu ribbon sample. Since this inelastic strain range determines the low cycle fatigue life of the joint, this reduction can become a benefit in enhancing the life of the solder.

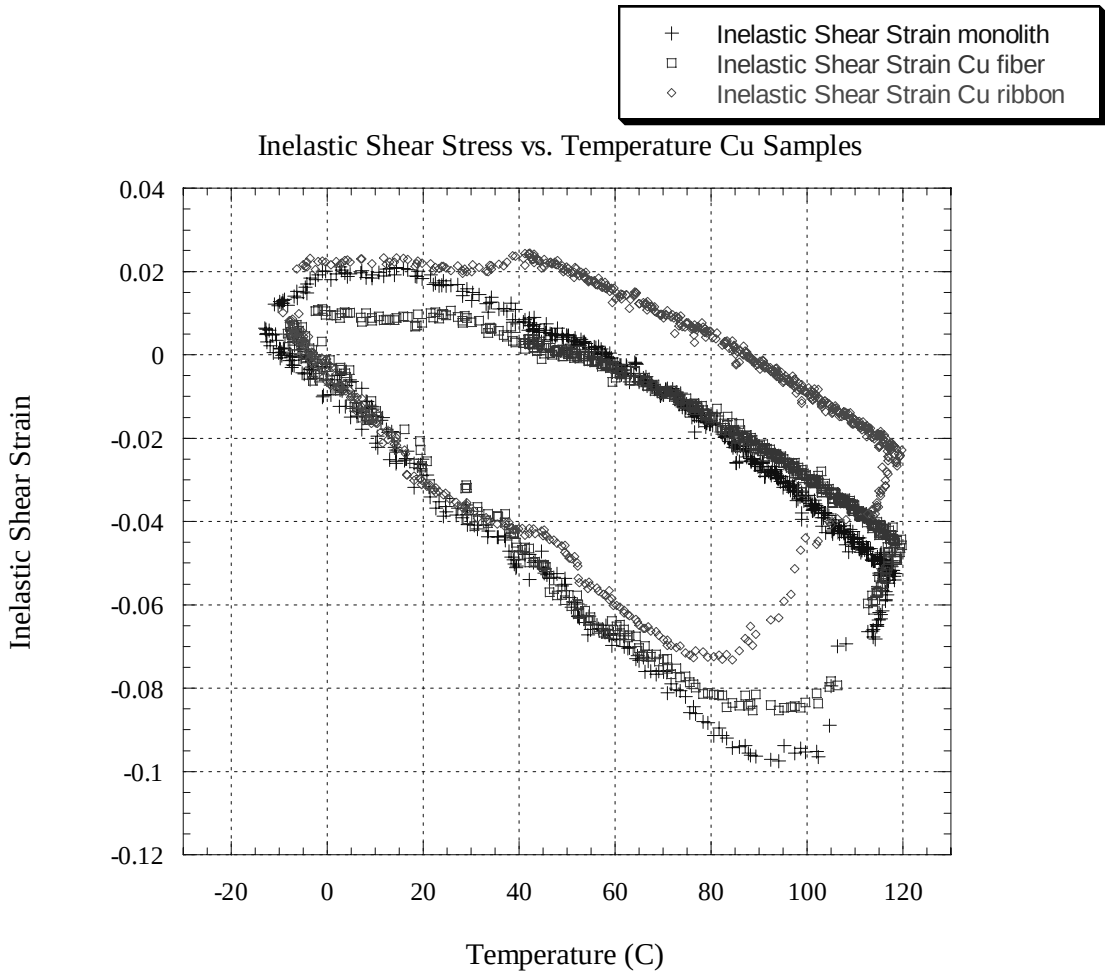

Figure 29. Inelastic Shear Strain vs. Temperature Plot for Cu Samples.

3. Monolithic vs. NiTi Fiber and NiTi Ribbon Samples

Two additional samples were prepared by Evangelos Fountoukidis and thermally cycled five times between two temperature extremes (-15 ^{o}C and 120 ^{o}C) to observe the material properties of active fiber reinforcements, NiTi SMA alloy.

As proposed earlier, mitigating the effects of strain localization within the joint, specifically at the solder/bond pad interfaces, can improve the performance of solder bonds and increase the chip life.

Figure 30 shows an experimentally obtained plot of the average joint shear stress (τ) versus temperature (T) during the 5th cycle for a monolithic cylinder solder, a NiTi fiber reinforced solder and a NiTi ribbon reinforced solder. The monolithic sample can be seen to follow a behavior similar to the plot previously presented, that is, the

measurement starts with the joint in an almost free state and stresses build up elastically until creep mechanisms start to operate, and beyond a certain point the plot shows non-linearity associated with stress relief due to creep. During cooling, the stresses build up again and below a certain temperature the joint is subjected to significant inelastic strains.

During the heating part of the cycle, figure 30 shows that the stresses are slightly built up more rapidly in the two samples which contain the NiTi fibers at the B2 temperature of each type of fiber (40 ^{o}C for the cylinder fiber and 80 ^{o}C for the ribbon fiber). At this martensite to austenite transformation temperature, the plots suffer a sudden change and the stress is slightly lowered.

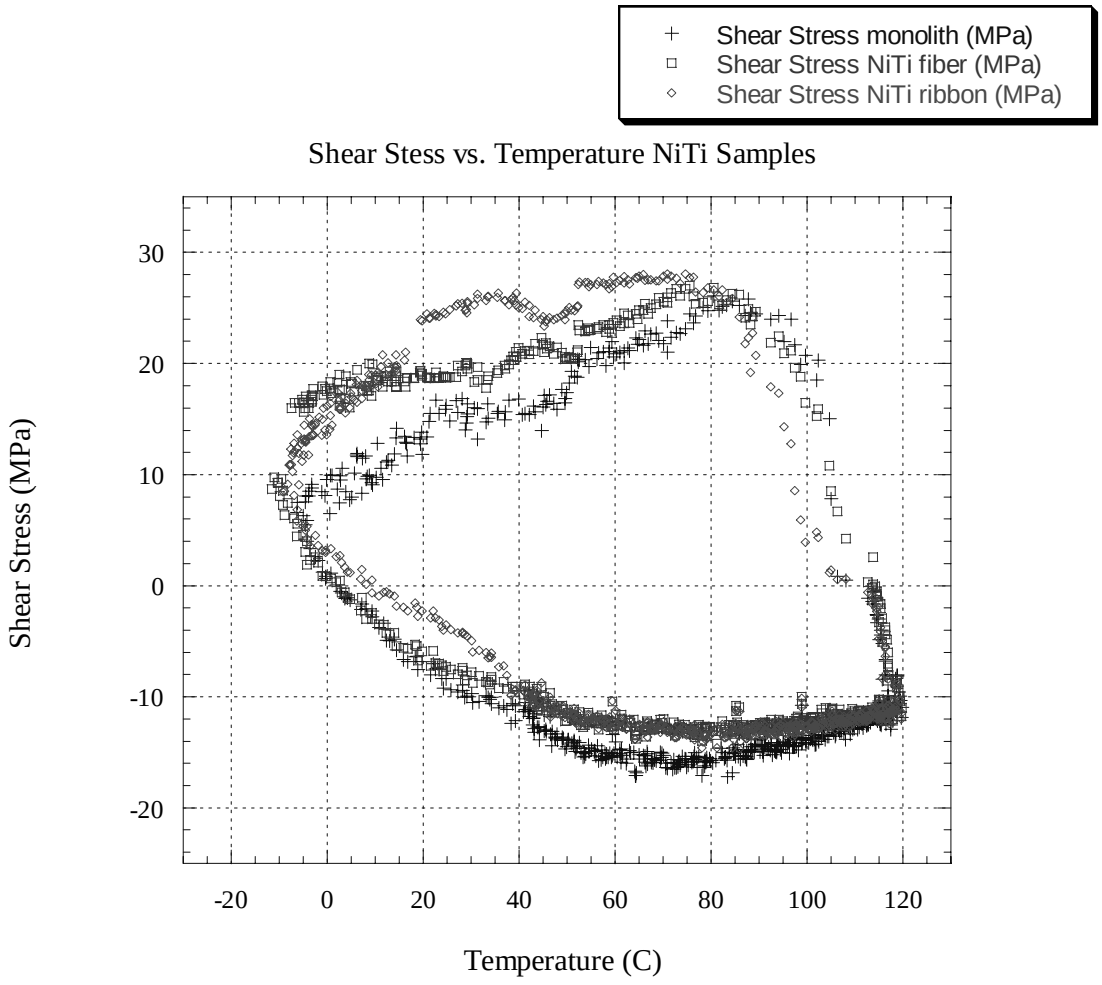

Figure 30. Shear Stress vs. Temperature Plot for NiTi Samples.

Figure 31 is a plot of the average inelastic shear strain ($\gamma_{inelastic}$) versus temperature during the 5th cycle for the same samples. Inelastic strain hysteresis is due to the operation of creep and plastic yielding. The $\Delta\gamma_{inel}$ for the monolithic solder is 0.117, 0.099 for the NiTi fiber reinforced solder and 0.095 for the NiTi ribbon reinforced solder. The total decrease in the inelastic strain range was 15.4% for the NiTi fiber sample and 18.8% for the NiTi ribbon sample. The figure details a much slower inelastic strain build up with a smaller change in the curve slope, indicating a reduction in the inelastic strain, which has been built up. Since this inelastic strain range determines the low cycle fatigue life of the joint, this reduction can become a benefit in enhancing the life of the solder. On the other hand, the increase in shear stress range implies that this extra stress is transferred to the Si chip. The Si chip is the most brittle part of the electronic device and can be severely affected.

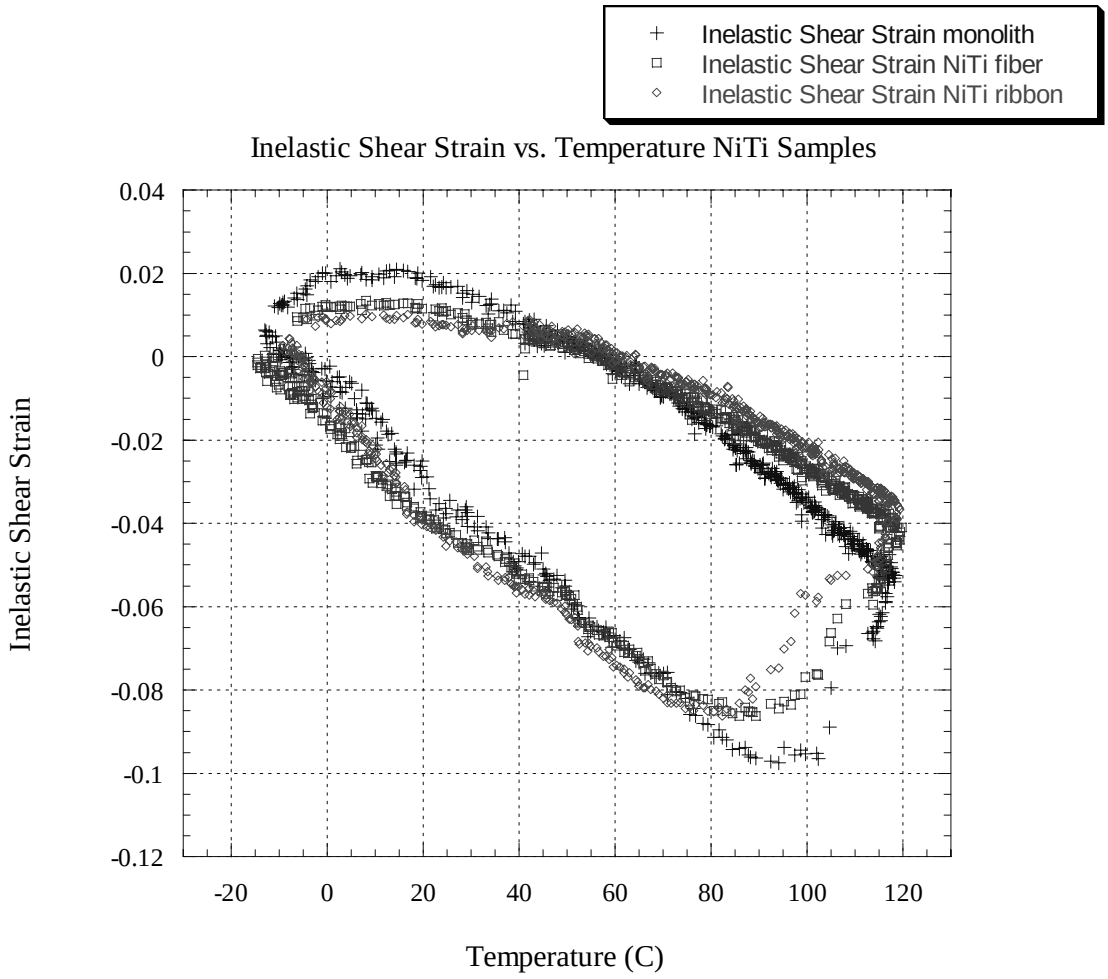

Figure 31. Inelastic Shear Strain vs. Temperature Plot for NiTi Samples.

C. NITI PARTICLES REINFORCED SOLDER

1. Solder Preparation

The composite solder of Sn-Ag-Cu was prepared by the following procedure. The starting materials were 95.5Sn-3.8Ag-0.7Cu powder (size range between 40µm and 50µm) matrix and NiTi particle (less than 38 µm) reinforcements. The composite solder, with a weight proportion of 10% of NiTi, was prepared by powder metallurgical route. The solder powder and NiTi particles were pre-weighed and then mechanically mixed together using a blender at 50 rpm for 60 minutes. The mixed powder was cold compacted at 25 MPa for 20 minutes ant then sintered at 210 ^{o}C for 12 hours.

2. Microstructure

The microstructural characterization of the Sn-Ag-Cu reinforced solder was carried out using a Jenaphot 2000 optical microscope. The standard metallographic procedures were used to prepare the smooth polished specimens for the microstructural evaluation.

Figures 32, 33 and 34 show the resulting microstructures at 290x, 750x and 1500x respectively. As observed here, the microstructure consists of a fine needle dispersion of Ag_3Sn (and some Cu_6Sn_5) precipitants in a β-Sn matrix and the NiTi particles embedded in this matrix. The next step would be to extrude this reinforced solder to plastically deform the solder in order to break the oxide layers and eliminate some minor voids around the NiTi particles.

Figure 32. 290x Optical Microscopy NiTi Powder Reinforced Solder.

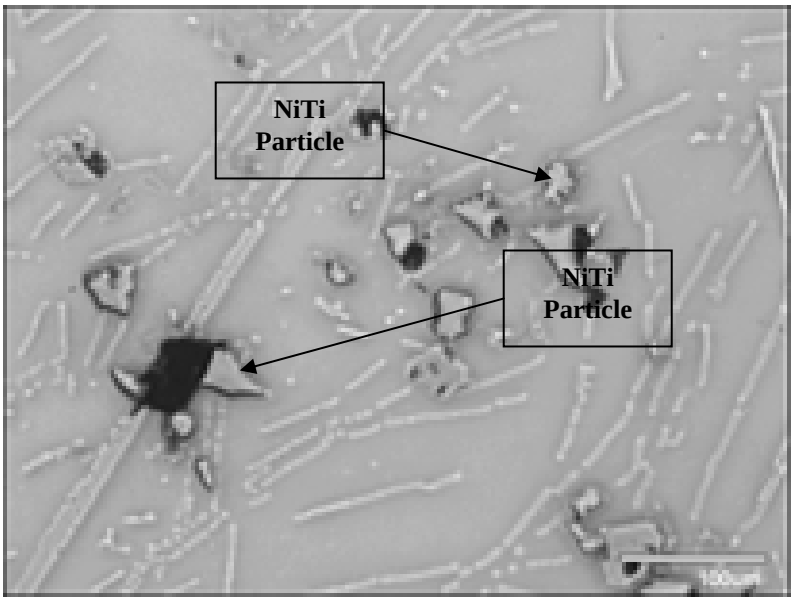

Figure 33. 370x Optical Microscopy NiTi Particles Reinforced Solder.

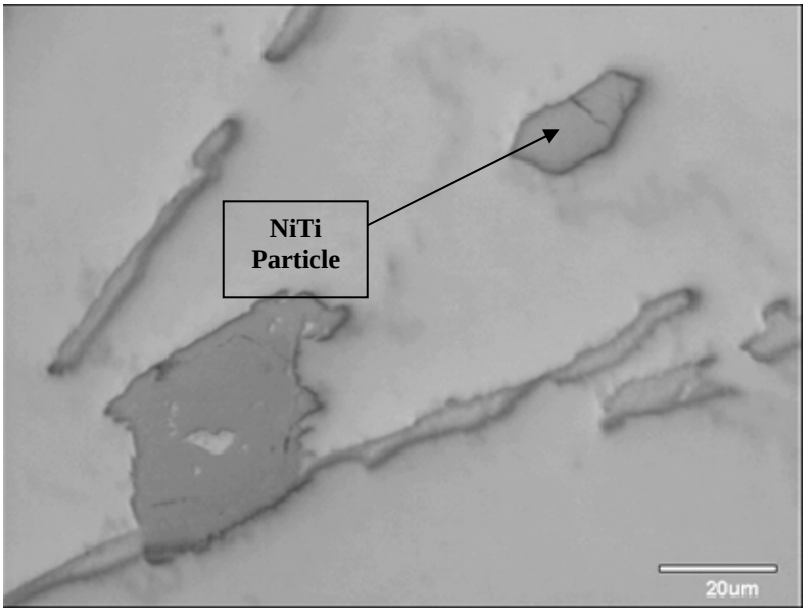

Figure 34. 1500x Optical Microscopy NiTi Particles Reinforced Solder.

V. SUMMARY

In this study, the effects of two shapes of Cu fibers of on the thermomechanical behavior of Sn-Ag-Cu solder were investigated and compared with the effects of NiTi SMA reinforcements. Samples for thermomechanical cycling tests were manufactured and thermally cycled. As expected, the effects of the addition of Cu fibers on the inelastic strain range were pronounced, but the shear stress range increased a considerable amount. Active reinforcements, like the NiTi fibers, produce the same effect on the strain range, almost without affecting the shear stress range.

NiTi SMA deforms in shear concurrently with the solder during the thermo-mechanical cycle, and subsequently undergoes strain recovery through martensite to austenite transformation, thereby placing the solder matrix next to the reinforcement in reverse shear and reducing the inelastic strain localization and the creep rate within the solder. This behavior can enhance the joint life. The total decrease in the inelastic strain range was 15.4% for the NiTi fiber sample and 18.8% for the NiTi ribbon sample, without enhancing the resultant stress range.

NiTi powder (~ 35μm) has been successfully produced from commercially available wire, by electrolytic hydrogen charging of a NiTi wire cathode to produce embrittlement, followed by a manual grinding to produce particles. The NiTi particles were mixed with the Sn-Ag-Cu solder powder in order to form a composite solder. Investigation of the cross section of the resultant solder has shown some segregation of the NiTi particles in clusters within the solder disc. Post-consolidation deformation processing is necessary to homogenize the particle distribution.

THIS PAGE INTENTIONALLY LEFT BLANK

LIST OF REFERENCES

1. Lau, John H., Donald W. Rice, “Solder Joint Fatigue in Surface Mount Technology: State of the Art,” Solid State Technology, pp. 91-104, October 1985.

2. Kloeser, Joachim, Erik Jung, Katrin Heinricht, Kai Kutzner, Andreas Ostmann and Herbert Reichl, “Reliability Investigations of Sn/Pb and Lead Free Solders for Flip Chip Technology,” Proceedings of Pan Pacific Microelectronics Symposium, pp. 93-102, 1998.

3. Frear, D. R., Dennis Grivas, and J. W. Morris Jr., “Thermal Fatigue in Solder Joints,” Journal of Metals, pp. 18-22, June 1988.

4. Anastacio, Onofrio A., “An Approach for Impression Creep of Lead Free Microelectronic Solders,” Center For Material Science and Engineering, Department of Mechanical and Astronautical Engineering, Naval Postgraduate School, 2002.

5. Crocker, Elroy S., “Effect of Cooling rates on the Microstructure of Bulk Sn-Ag Solder,” Center For Material Science and Engineering, Department of Mechanical and Astronautical Engineering, Naval Postgraduate School, 2003.

6. Lee, Y. G., J. G. Duh, “Characterizing the Formation and Growth of Intermetalic Compound in the Solder Joint,” Journal of Material Science, 33, pp. 5569-5572, 1998.

7. “The International Technology Roadmap for Semiconductors,” Semiconductor Industry Association, San Jose, CA, 1999.

8. Frear, D. R., Dennis Grivas, and J. W. Morris Jr., “A Microstructural Study of the Thermal Fatigue failures of 60Sn-40Pb Solder Joints,” Journal of Electronic Materials, Vol. 17, No. 2, pp. 171-180, 1998.

9. Hacke, P., A. Sprecher, and H. Conrad, “Microstructure Coarsening During Thermo-Mechanical Fatigue of Pb-Sn Solder Joints,” Journal of Electrinic Materials, Vol. 26, No. 7, 1997.

10. Conrad, H., Z. Guo, Y. Fahmy, and Di Yang, “Influence of Microstructure Size on the Plastic Deformation Kinetics, Fatigue Crack Growth Rate, and Low Cycle Fatigue of Solder joints,” Journal Of Electronic Materials, Vol. 28, No. 9, 1999.

11. Hacke, P. L., Y. Fahmy, and H. Conrad, “Phase Coarsening and Crack Growth Rate During Thermo-Mechanical Cycling of 63Sn-37Pb Solder Joints,” Journal of Electronic Materials, Vol. 27, No. 8, 1998.

12. Frear, D. R., “The Mechanical Behavior of Interconnect Materials for Electronic Packaging,” JOM, pp. 49-53, May 1996.

13. Masazumi Amagai et al, “Mechanical Characterization of Sn-Ag-based Lead-Free Solders,” Microelectronics Reliability, Vol. 42, pp. 951-966, 2002.

14. Guo, F., J. Lucas, and K. N. Subramanian, “Creep behavior in Cu and Ag Particle-Reinforced Composite and Eutectic Sn-3.5Ag and Sn-4.0Ag-0.5Cu Non-Composite Solder Joints,” Journal of Materials Science: Materials in Electronics, 12, pp. 27-35, 2001.

15. F. Guo et al, “Microstructural Characterization of Reflowed and Isothermally-Aged Cu and Ag Particulate Reinforced Sn-3.5Ag Composite Solders,” Soldering and Mount Technology, 13/1, pp. 7-18, 2001.

16. Seong-Yong Hwang et al, “Microstructure of Lead-Free Composite Solder Produced by an In-Situ Process,” Journal of Electronic Materials, Vol. 31, No. 11, pp. 1304-1308, 2002.

17. McDougall, J., S. Choi et al, “Quantification of Creep Strain Distribution in Small Crept Lead-Free In-Situ Composite and Non-Composite Solder Joints,” Materials Science and Engineering, A285, pp. 25-34, 2000.

18. C. G. Kuo et al, “Creep-Fatigue Life Prediction of In-Situ Composite Solder Joints,” Metallic Materials Transactions, 26A, pp. 3265-3272, 1995.

19. Silvain, J. F., J. Chazelas, M. Lahaye and S. Trombert, Materials Science and Engineering, A273-275, pp. 818-826, 1999.

20. Walsh, John P., “The Effects of Coarsening in 96.5Sn-3.5Ag Solder Joints during Isothermal Annealing and Thermomechanical Cycling,” Center For Material Science and Engineering, Department of Mechanical and Astronautical Engineering, Naval Postgraduate School, March 2004.

21. Dutta, Indranath, A. Gopinath and C. Marshall, “Underfill Constraint Effects during Thermomechanical Cycling of Flip Chip Solder Joints,” Journal of Electronic Materials, Vol. 31, No. 4, 2002.

22. Wright, William L., “Processing of NiTi Reinforced Adaptive Solder for Electronic Packaging,” Center For Material Science and Engineering, Department of Mechanical and Astronautical Engineering, Naval Postgraduate School, March 2004.

23. SChoi, S., K.N. Subramanian et al, “Effect of Cooling Rate on Microstructure and Mechanical Properties of Eutectic Sn-Ag Solder Joints with and without Intentionally Incorporated Cu_6Sn_5 Reinforcements,’ Journal of Electronic Materials, Vol. 28, No. 11, pp. 1184-1197, 1999.

24. Dutta, Indranath, “A Constitutive Model for Creep of Lead Free Solders Undergoing Strain Enhanced Microstructural Coarsening: A First Report,” Journal of Electronic Materials, Vol. 32, No. 4, 2003.

25. D. Lewis et al, “Determination of the Eutectic Structure in the Ag-Cu-Sn System,” Journal of Electronic Materials, Vol. 31, No. 2, 2002.

26. Frear, S., Burchet, M. Neilsen and J. Stephens, “Microstructurally Based Finite Element Simulation of Solder Joint Behavior,” Soldering and Surface Mount Technology, No. 25, 1997.

27. Gibson, A., S. Choi, K. Subramanian and T. Bieler, “Issues Regarding Microstructural Coarsening Due to Aging of Eutectic Tin-Silver Solder,” Department of Material Science and Mechanics, Michigan State University, 1997.

28. Hacke, P., A. Sprecher and H. Conrad, “Modeling of the Thermomechanical Fatigue of 63Sn-37Pb Alloy,” Material Science and Engineering Department, North Carolina State University, 1998.

29. Plumbridge, W. J., “Materials Behavior and the Reliability in Performance of Solder Joints,” Soldering and Surface Mount Technology, 11/3, pp. 8-11, 1999.

30. R. Darveaux et al, “Constitutive Relations for Tin-Based Solder Joints,” IEEE Transactions on Components, Hybrids, and Manufacturing Technology, Vol. 15, No. 6, pp. 1013-1024, December 1992.

31. J. P. Lucas et al, “Creep Deformation Behavior in Eutectic Sn-Ag Solder Joints Using a Novel Mapping Technique,” Journal of Electronic Materials, Vol. 28, No. 11, pp. 1270-1275, 1999.

32. Glazer, J., “Metallurgy of Low Temperature Pb-Free Solders for Electronic Assembly,” International Materials Reviews, Vol. 40, No. 2, pp. 65-75, 1995.

33. C. H. Reader et al, “Isothermal Creep of Eutectic SnBi and SnAg Solder and Solder Joints,” IEEE/CPTM International Manufacturing Technology Symposium, pp. 1-6, 1994.

34. P. L. Tu et al, “Effects of Intermetallic Compounds on the Thermal fatigue of Surface Munt Solder Joints,” IEEE Transactions of Components, Packaging, and Manufacturing Technology, Vol. 20, No. 8, pp. 757-764, August 1994.

35. Rhee, H., F. Guo, J. Lee, K. Chen and K. Subramanian, “Effects of Intermetallic Morphology at the Metallic Particle/Solder Interface on Mechanical Properties of Sn-Ag-Based Solder Joints.

36. H. Betrabet et al, “Processing Dispersion-Strengthened Sn-Pb Solders to Achieve Microstructural Refinement and Stability,” Vol. 25, pp. 2323-2328, 1991.

37. McCormack, M., S. Jin, and G. Kammlott, “Enhanced Solder Alloy Performance by Magnetic Dispersions,” IEEE Transactions on Components, Packaging, and Manufacturing Technology, Vol. 17, No. 3, pp. 452-457, September 1994.

38. Choi, S., J. Lee et al, “Creep Properties of Sn-Ag Solder Joints Containing Intermetallic Particles,” Journal of Electronic Materials, pp. 22-26, June 2001.

39. Guo, F., J. Lee et al, “Processing and Aging Characteristics of Eutectic Sn-3.5Ag Solder Reinforced with Mechanically Incorporated Ni Particles,” Journal of Electronic Materials, Vol. 30, No. 9, pp. 1073-1082, 2001.

40. Dutta, Indranath, B. Majumdar, D. Pan, W. Horton, W. Wright, and Z. Wang, “Development of a Novel Adaptive Lead-Free Solder Containing Reinforcements Displaying the Shape Memory Effect,” Electronic Mater, November 2003.

41. Dutta, Indranath, C. Park, S. Choi, “Impression Creep Characterization of Rapidly Cooled Sn-3.5Ag Solders,” materials Science Engineering, 2003.

42. Fang, T., Wiley Encyclopedia of Electrical and Electronic Engineering, Vol.1, 128.

THIS PAGE INTENTIONALLY LEFT BLANK

INITIAL DISTRIBUTION LIST

1. Defense Technical Information Center
   Ft. Belvoir, Virginia

2. Dudley Knox Library
   Naval Postgraduate School
   Monterey, California

3. Professor Indranath Dutta
   Mechanical and Astronautical Engineering
   Naval Postgraduate School
   Monterey, California